UNIVERSITÀ DEGLI STUDI DI MILANO

PhD course of

Integrated Biomedical Research

Cycle XXXI

BIO-09

"The transcription factor NFIX as a novel modulator of heart rate."

Sara Landi

R11322

Tutor: Prof. Andrea Francesco Barbuti

PhD Course Coordinator: Prof. Chiarella Sforza

2017/2018

Summary

Abstract 4

Introduction 6

1. The transcription factor NFIX. 6

2. Heart development. 13

3. The Heart. 18

I. The Working Myocardium. 18

II. The Conduction System 18

4. The Cardiac Action Potential. 24

5. HCN Channels. 27

6. L-type Calcium Channels. 32

Aim 37

Materials and methods 38

1. Statistical Analysis 38

2. Mouse model 38

3. RNA Extraction and Retrotranscription 39

4. qPCR and RNA sequencing 41

5. Histological Analysis 44

6. In vivo Telemetry 45

7. Isolation of Sinoatrial Node Cells (SANCs) 46

8. Isolation and Infection of neonatal rat ventricular cardiomyocytes (NRVCs) 47

9. Electrophysiology 48

Results 50

1. Nfix expression in the heart 50

I. Nfix gene expression during cardiac development. 50

II. Nfix gene expression in the adult heart. 50

2. Cardiac morphology of WT and **Nfix***-null mice* 52

3. NFIX loss increases intrinsic heart rate. 55

4. NFIX loss enhances CAV1.3- L-Type Calcium current but does not affect Funny current. 60

Discussion 64

References 70

Abstract

NFIX is a transcription factor involved in the development of various organs among which the brain and the skeletal muscle. In the skeletal muscle, NFIX induces the switch from embryonic to fetal myogenesis and it regulates the regeneration process in the adult mouse. Considering that skeletal and cardiac muscle share several signaling pathways beyond the same mesodermal origin, here we investigated for the first time the expression profile and role of NFIX in the heart.

We discovered that *Nfix* gene is barely expressed at early stages of heart development but its expression increases after birth until postnatal day 7. Histological analysis revealed no apparent morphological alterations *Nfix*-null hearts when compared to WT littermates. In agreement with these data, no differences in the expression of the sarcomeric genes such as cardiac myosins (*Myh6, Myh7, Mlc2v*), troponin (*cTnI*) and of the transcription factor *Nkx2.5* were found between WT and *Nfix*-null mice. In the adult heart, *Nfix* gene is highly expressed in both atria and ventricles but significantly less expressed in the sinoatrial node (SAN) where the heart rhythm originates. Electrocardiograms recordings in freely moving mice show that *Nfix*-null mice (523.10±13.25 bpm, n=4) present tachycardia compared to WT mice (466.98±8.42 bpm, n=5). Isolated SAN cardiomyocytes from *Nfix*-null mice display a higher intrinsic heart rate (577.80±52.80 bpm, n=7) than WT cells (403.80±45.00 bpm, n=7) suggesting that *in vivo* tachycardia is not caused by a dysregulation of autonomic nervous system. Using RNA interference, we silenced *Nfix* gene in neonatal rat ventricular cardiomyocytes (NRVCs) and confirmed a +62.2% increase in action potential rate in *Nfix*-silenced (87.60±7.80 bpm, n=20) compared to scrambled NRVCs (54.00±9.00 bpm, n=19). It is well established the role of

pacemaker currents (funny current and calcium currents) in setting action potential rate. We did not find differences in funny current between *Nfix*-silenced versus control NRVCs and in *Nfix*-null versus WT SAN cells, but we demonstrated an increase of L-type calcium current in *Nfix*-silenced NRVCs compared with the control. In line with these functional data, we found a higher expression of *Cacna1d*-mRNA in *Nfix*-null SAN than in WT SAN according with a possible increase of CaV1.3 L-type calcium channel density.

In conclusion, our data suggest that NFIX acts as negative modulator of the heart rate probably affecting L-type calcium current; however, further analysis are necessary to properly clarify the molecular pathway in which NFIX acts.

Introduction

1. The transcription factor NFIX.

NFIX is a transcription factor involved in the development of various organs. It belongs to the *Nuclear Factor I* (NFI) transcription factor family together with NFIA, NFIB and NFIC in vertebrates. In mouse, *Nfix* gene is located on chromosome 8 from nucleotide 84699876 to 84800344 and it encodes for a protein of ≈48 kDa. NFI proteins bind as a dimer the dyad symmetric consensus sequence TTGGC(XXXXX)GCCAA on duplex DNA (Gronostajski et al., 2000). Each *Nfi*-mRNA can be alternatively spliced generating multiple proteins that conserve some functional domains (Figure 1):

- The ***N-terminus*** contains the highly conserved DNA binding/dimerization domain (200 amino acids in length). It does not show homology in sequence with other known DNA-binding domains revealing a unique structure for NFI protein. The N-terminal portion is sufficient for the DNA binding and dimerization activity, and it is able to activate DNA replication in adenovirus (Mermod et al., 1989, Gounari et al., 1990). In particular, it has been shown that the deletion or the mutation of four cysteine residues makes the NFI protein non-functional (Guehmann et al., 1992).
- The ***C-terminus*** contains the domains related to the modulation of target genes by NFI proteins. It presents a Proline-rich domain that is able to stimulate the transcription of genes in mammalian cells. On the other hand, NFI proteins are also able to inhibit mRNA transcription; NFI regulatory elements have been identified into silencers regions of several transcripts such as peripherin, alpha1B adrenergic receptor and GLUT4 genes (Gronostajski et al., 2000).

In the mouse, NFI genes are expressed in several tissues (Figure 2A): *Nfia* and *Nfib* mRNAs are abundant in heart and lung and they are both expressed in liver, skeletal muscle and brain. *Nfic* and *Nfix* transcripts display a similar expression pattern: they are expressed in skeletal muscle at higher levels than in heart, liver, kidney, lungs and brain. All *Nfi*-mRNA have a low expression in spleen and testis (Chaudry et al., 1997). During embryonic development in mouse, it was shown by *in situ* hybridization experiments, that *Nfia* is the first transcript detected at day 9 *post coitum* (9 dpc) in the heart and in the *septum transversum*. At 10.5 dpc, *Nfib*-mRNA is detected in developing lungs, while *Nfic* in the aortic arches. Only at 11.5 dpc, all *Nfi* transcripts start to be found with an overlapping expression pattern (Figure 2B); *Nfi* genes are highly expressed in brain and in the neural tube. In the liver and in skeletal muscle, the main isoform is *Nfix*. At 12.5-14.5 dpc it is possible to find *Nfix*, *Nfia* and *Nfic* in developing skeletal muscles, and *Nfix* and *Nfib* in the migrating neurons of the spinal cord and cerebellum. In the postnatal brain, all the *Nfi* transcript isoforms are expressed and maintained until adulthood (Figure 2C). In particular, *Nfix* is expressed in the grey matter, the hippocampus and in the dentate gyrus (Chaudry et al., 1997).

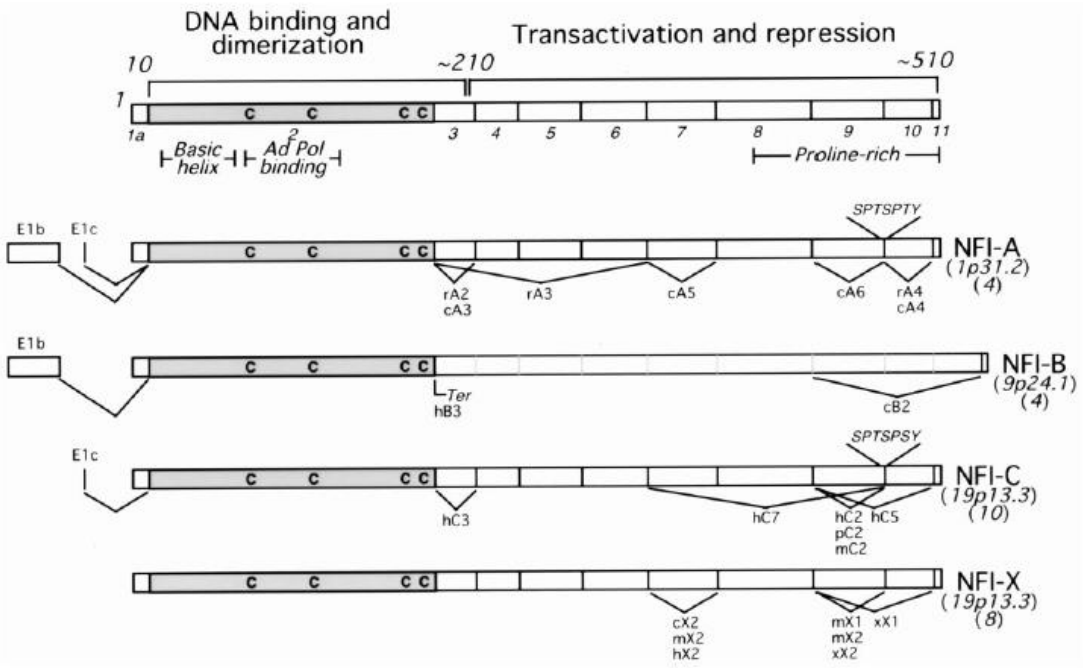

Figure 1. Domains and alternative splicing of NFI genes in vertebrates. From Gronostajski et al., 2000.

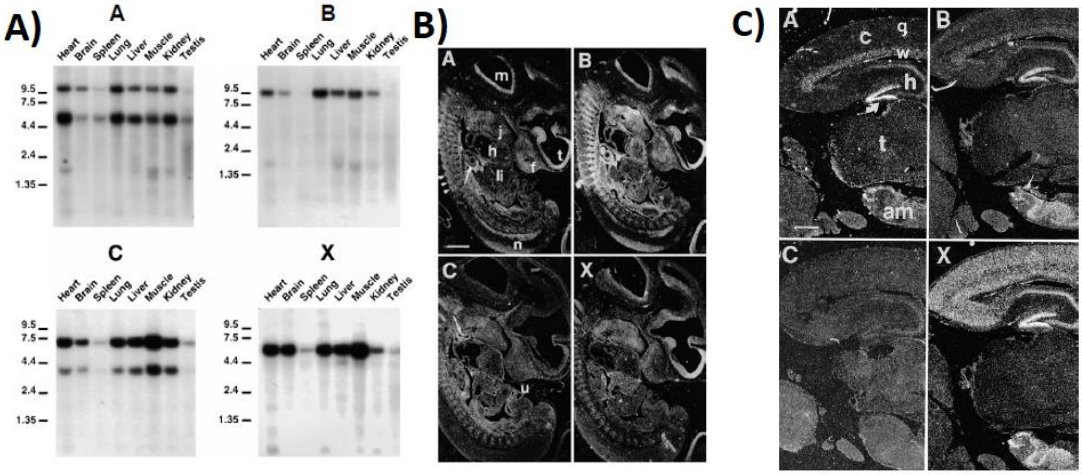

Figure 2. A) NFI transcripts detection in heart, brain, spleen, lung, liver, skeletal muscle, kidney and testis in mice. B) Nfi mRNA localization at 11.5 dpc. A= Nfia; B= Nfib; C= Nfic; X= Nfix. C) Nfi mRNA localization in the postnatal brain. From Chaudry et al., 1997.

In order to elucidate the role of NFI proteins, several transgenic mouse models have been generated:

- ***Nfia* Knock-out** (KO): the majority of mice die at birth (das Neves et al., 1999); they show a delayed neuronal development (Piper et al., 2010) and defects in hydrocephalus (das Neves et al., 1999).
- ***Nfib* KO** mice die at birth (Grunder et al., 2002) and display several defects in central nervous system (CNS) (Barry et al., 2008, Betancourt et al., 2014) and lung hyperplasia.
- ***Nfic* KO** mice are viable but present defects in tooth development.
- ***Nfix* KO** mice generally die around 3-4 weeks after birth. They display defects in sympathetic nervous system (Piper et al., 2011) and skeletal muscle development (Messina et al., 2010, Driller et al., 2007).

Recently, the role of NFIX in the brain has been elucidated (Campbell et al., 2008, Driller et al., 2007). During brain development, NFIX is essential in neural progenitors commitment (Harris et al., 2016), regulating the specific timing of differentiation of neurons and astrocytes. NFIX is able to inhibit the expression of the transcription factor *Sox9*, essential in cortical stem cells renewal, resulting in an upregulation of SOX9 in *Nfix* KO mice (Vidovic et al., 2015). Furthermore, NFIX helps the development of the ependymal cells in the lateral ventricles through *Foxj1* activation (Vidovic et al., 2018). In the spinal cord gliogenesis, NFIX participate downstream to the program activated by both NFIA and NFIB unrevealing a regulatory network between NFI proteins (Matuzelski et al., 2017). On the other side, recent studies demonstrated that NFIX has a pivotal role in the skeletal muscle (Messina et al., 2010, Rossi et al., 2016) (Figure 3, A). During skeletal myogenesis, PAX7 directly activates the *Nfix* expression in the transcriptional switch

from embryonic to fetal fibers. Specific *knock-out* of *Nfix* gene in the skeletal muscle obtained from crossing *Nfix*:loxP$^{+/+}$ and *MyoD*:Cre Recombinase mice displayed a severe disorganization of muscle fibers in the fetus (Figure 3, C) but they are indistinguishable from WT at earlier stages of development (Messina et al., 2010). Indeed, NFIX is necessary for the simultaneous activation of the fetal-specific promoters (such as *Mck* and β-enolase) and the inactivation of embryonic promoters (slow myosin, *slowMyHC*) in the fetus (Figure 3, B). NFIX must associate with MEF2A and PKCθ on *Mck* promoter to activate gene transcription. Furthermore, NFIX represses *MyHC-I* promoter during the fetal myogenesis (Taglietti et al., 2016). In the adult mice, the loss of function of NFIX causes a delay in muscle regeneration after injury: NFIX indeed silences *Myostatin* promoter in satellite cells, a condition that is necessary for starting the regeneration process (Figure 3, D). Recently, *Nfix* silencing has been proposed as an innovative therapeutic strategy to delay the regeneration process in the dystrophic muscle to inhibit the pathological process (Rossi et al., 2017).

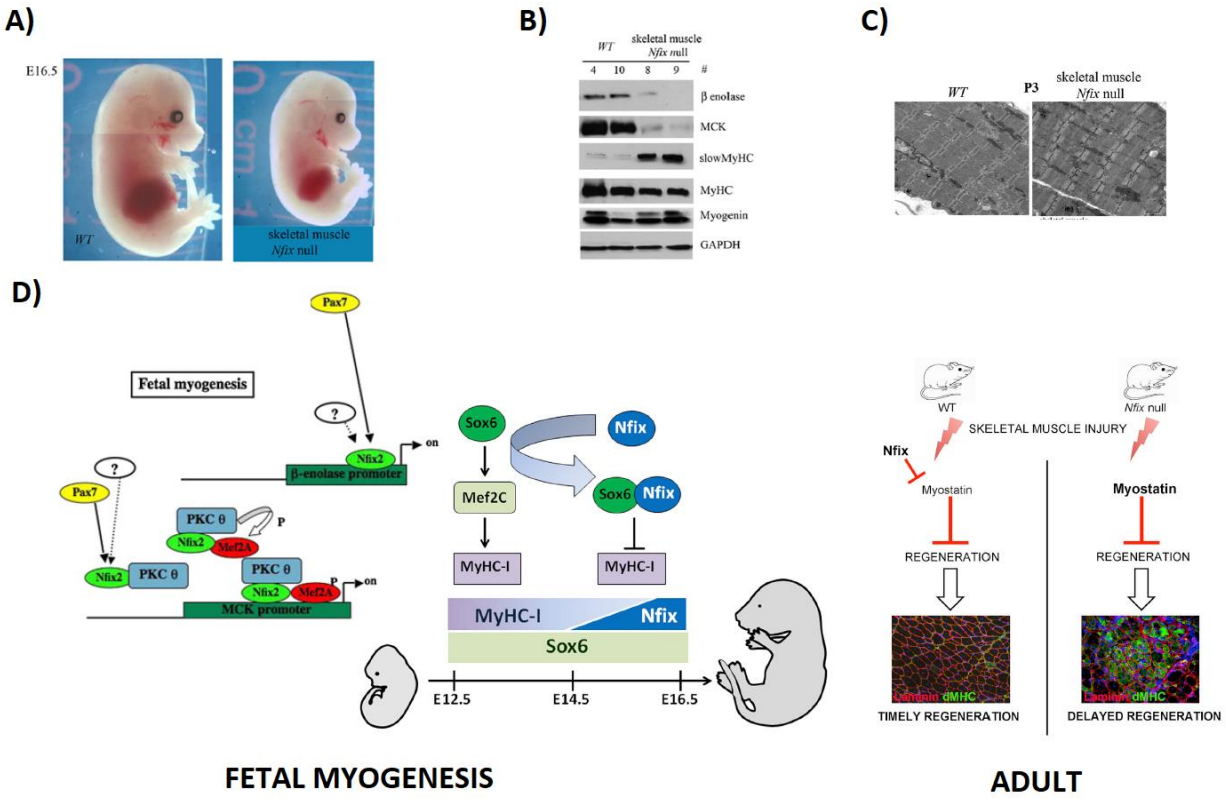

Figure 3. A) Morphology of WT and skeletal muscle specific Nfix*-deficient mouse (MyoD:Nfix) at embryonic day 16.5. B) Protein expression of embryonic (slowMyHC) and fetal markers (βenolase, MCK) in skeletal muscle* Nfix*-null and WT. C) Transverse section of hind limbs acquired using transmission electron microscopy (TEM) of WT and skeletal muscle specific* Nfix*-deficient mouse at E16.5. D) Schematic illustration of NFIX network during fetal myogenesis and in the skeletal muscle in the adult. Modified from Messina et al., 2010, Taglietti et al., 2016, Rossi et al., 2016.*

Alterations of *NFIX* gene expression have been reported in human diseases such as cancer and overgrowth diseases (Rahman et al., 2017, Liu et al.,2017, Kleemann et al., 2018, Malan et al., 2010). *Loss-of-function* mutations in *NFIX* gene have been associated with two autosomal overgrowth disorders, *Malan* and *Marshall-Smith* Syndrome; they are rare diseases with an incidence of 1/1000000 and appear during childhood (Malan et al., 2010). Their phenotype resemble Nfix KO mouse model with anomalies in the

skeleton including kyphosis and reduced bone density. This evidence supports the use of Nfix KO animals as a suitable model of the pathology (Driller et al., 2007). Moreover, NFIX is expressed in the heart (Chaudry et al., 1997) and in some Malan Syndrome patients cardiovascular anomalies occur in the form of aortic dilatation (Priolo et al., 2018), but its role in cardiac physiology has not been elucidated yet.

2. Heart development.

In vertebrates, the heart derives from a group of mesodermal germ layer cells that differentiate into *mesothelium*, *endothelium*, and *myocardium*. Despite the fact that generally mammals display huge differences in the duration of gestation, mice and humans show a very similar sequence of events during cardiac development (Figure 4A and B) with minor differences in atrial and venous morphology, as demonstrated by Krishnan and colleagues (Figure 4C).

At the end of the gastrulation (around day 20 of human or day 8 of mouse development), heart development begins with the formation of two endocardial tubes (*right and left endocardial tubes*) which merge to form a single tubular structure, also called the "*primitive heart tube*". In human, around day 20-21 of development, the heart becomes the first functional organ in the embryo; it contracts spontaneously pumping the blood through the vessels (Moorman et al., 2003). Myocytes start to display a rhythmic electrical activity before the fusion of the endocardial tubes. The primitive heart tube is then organized into:

- the "*truncus arteriosus*" that will divide into aorta and pulmonary arteries;
- the "*bulbus cordis*" that will generate the right ventricle;
- the "*primitive ventricle*" acts as the initial pacemaker even if the pacemaker activity is actually made by a group of cells that derive from the sinus venous. It will then generate the left ventricle;
- the "*primitive atria*" that will generate the atria and their appendages;
- the "*sinus venous*", that is responsible for the blood circulation in the early stages of heart development. It will generates the posterior part of the right atrium, the sinoatrial node (SAN) and the coronary sinus.

A)

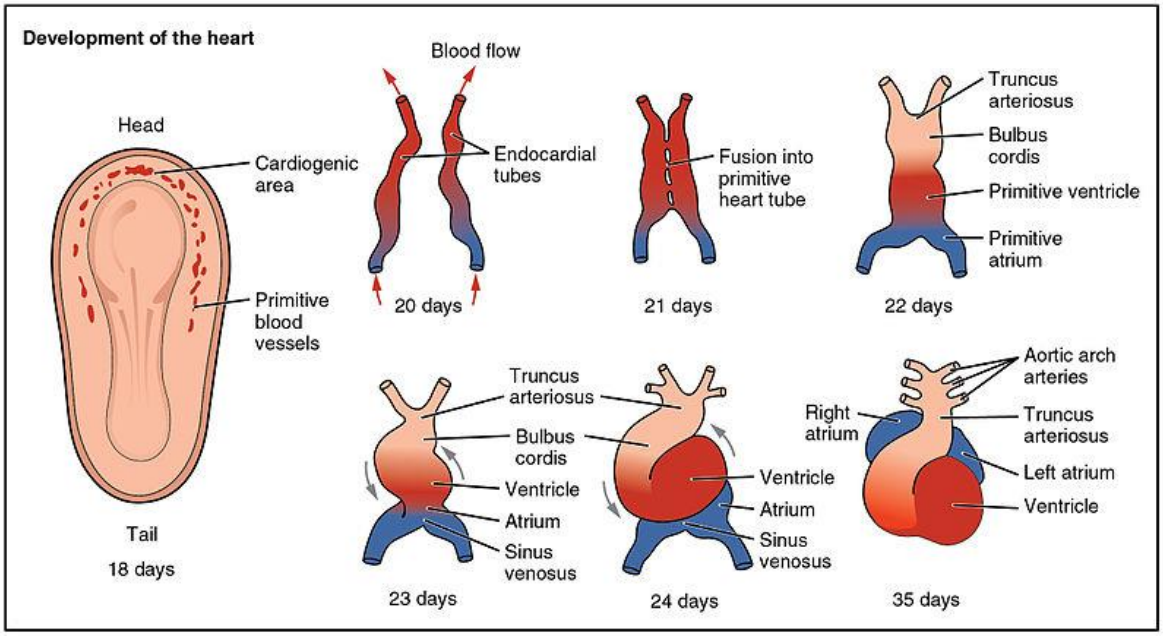
Development of the heart
Head
Cardiogenic area
Primitive blood vessels
Tail
18 days
Blood flow
Endocardial tubes
20 days
Fusion into primitive heart tube
21 days
Truncus arteriosus
Bulbus cordis
Primitive ventricle
Primitive atrium
22 days
Truncus arteriosus
Bulbus cordis
Ventricle
Atrium
Sinus venosus
23 days
Ventricle
Atrium
Sinus venosus
24 days
Aortic arch arteries
Right atrium
Truncus arteriosus
Left atrium
Ventricle
35 days

B)

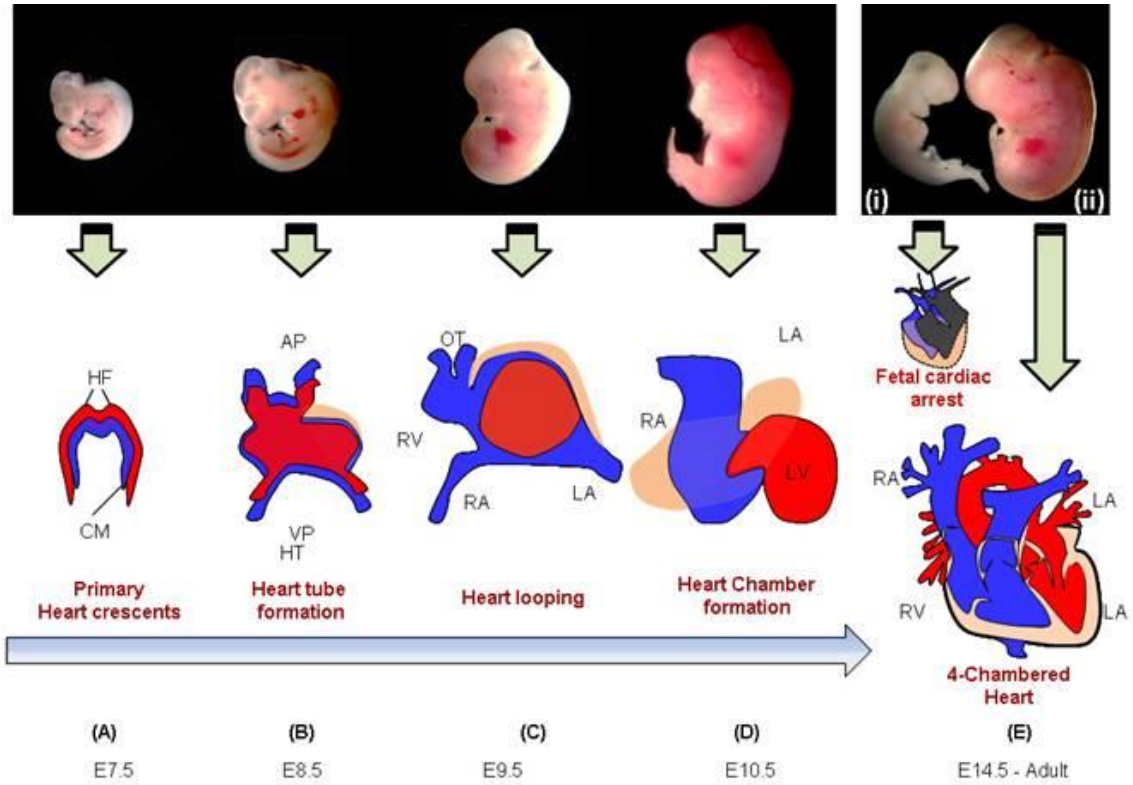
(i)
(ii)
HF
CM
AP
VP
HT
OT
RV
RA
LA
LA
RA
LV
Fetal cardiac arrest
RA
LA
RV
LA
Primary Heart crescents
Heart tube formation
Heart looping
Heart Chamber formation
4-Chambered Heart
(A)
E7.5
(B)
E8.5
(C)
E9.5
(D)
E10.5
(E)
E14.5 - Adult

C)

Parallel stages of cardiovascular development in mouse and human

Mouse Developmental Stage (E*)	Human Carnegie Stage	Human EGA (weeks)	Major morphogenetic events
9.5–10.5	13–17	6 4/7 – 7 5/7	Cardiac loop
11.5	15–16	7 1/7 – 7 3/7	Atrial septation, muscular interventricular septum formation, early outflow septation
12.5	CS 17–18	7 5/7 – 8	Atrial septation, outlet ventricular septum formation, beginning of semilunar valve formation
13.5	CS 19–CS 21	8 2/7 – 8 6/7	Completion of membranous/inlet ventricular septum formation
14.5	CS 22	9 1/7	All definitive major cardiac structures identifiable
15.5–17.5	CS 23	CS 23	Progressive myocardial compaction, AV and semilunar valve refinement
17.5-birth	No comparable stage	No comparable stage	Continued myocardial compaction, semilunar valve refinement

*E = days post conception

Figure 4. Schematic representation of embryonic cardiac developmental stages, growth and formation of four-chambered heart in humans (A) and mice (B). In panel C a parallelism of cardiovascular development between human and mice. Abbreviations: HF, Heart Fields; CM, Cardiogenic Mesoderm; AP, Arterial Pole; OT, Outflow Tract; HT, Heart Tube; VP, Venous Pole; RV, Right Ventricle; LV, Left Ventricle; RA, Right Atrium; LA, Left Atrium; PA, Pulmonary Artery; A; Aorta. Adapted from "Anatomy & Physiology", 2013 (A) and Krishnan et al., 2014 (B and C).

The primitive heart tube stretches until it loops and generates the four chambers and paired arterial trunks that form the adult heart in a process called "*cardiac looping*" (Moorman e Christoffels, 2003). The tube is divided into the cardiac regions along its cranio-caudal axis: the primitive ventricle ("*primitive left ventricle*") and the trabecular proximal arterial bulb ("*primitive right ventricle*").

As mentioned before, the sinus venous receives the venous blood from the poles of right and left sinus. Each pole receives blood from three major veins: the *vitelline vein*, the *umbilical vein* and the *common cardinal vein*. When the left common cardinal vein disappears in the tenth week, the right pole together with the right atrium generate the wall of the right atrium. The right and left venous valves merge and form the *septum spurium* that will develop into the inferior valve of the vena cava and the coronary sinus valve. SAN and the atrioventricular node (AVN) pacemaker cells originate from the primitive atrium and the sinus venous. Molecularly, SAN precursors are characterized by the specific expression pattern of transcription factors including TBX18, SHOX2 and ISL-1 (Mommersteeg et al., 2010, Hoogaars et al., 2004). NKX2.5 has a complementary expression pathway to TBX2 and SHOX2 that are required to activate the pacemaker program (Figure 5). Indeed, NKX2.5 transcription is blocked in SAN by SHOX2 but not in the myocardium chambers where it activates, together with TBX5, the myocardium promoters of *Nppa*, *Cx40* and *Cx43* genes (Hoogaars et al., 2007). The sinus venous is a symmetric structure but SAN originates only in the right atrium because of the presence of the transcription factor PITX2c that specifically suppresses the SAN program in the left region allowing the correct asymmetric development (Mommersteeg et al., 2007; Barbuti and Robinson 2015).

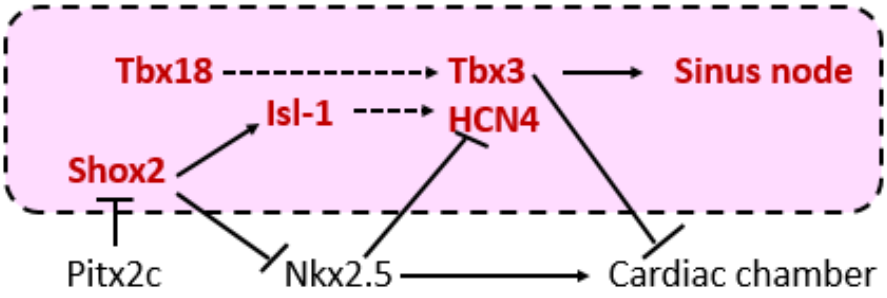

Figure 5. Schematic representation in sinus node specification. Modified from Barbuti and Robinson., 2015.

In the majority of the mammals, during cardiac development the heart rate is higher than in adulthood. In the first month of human development, embryonic heart rate (EHR) accelerates linearly peaking at 165-185 bpm in humans. During the 15th week, EHR decelerates to 150 bpm and then deceleration rate slows reaching an average rate of 145 bpm (Figure 6).

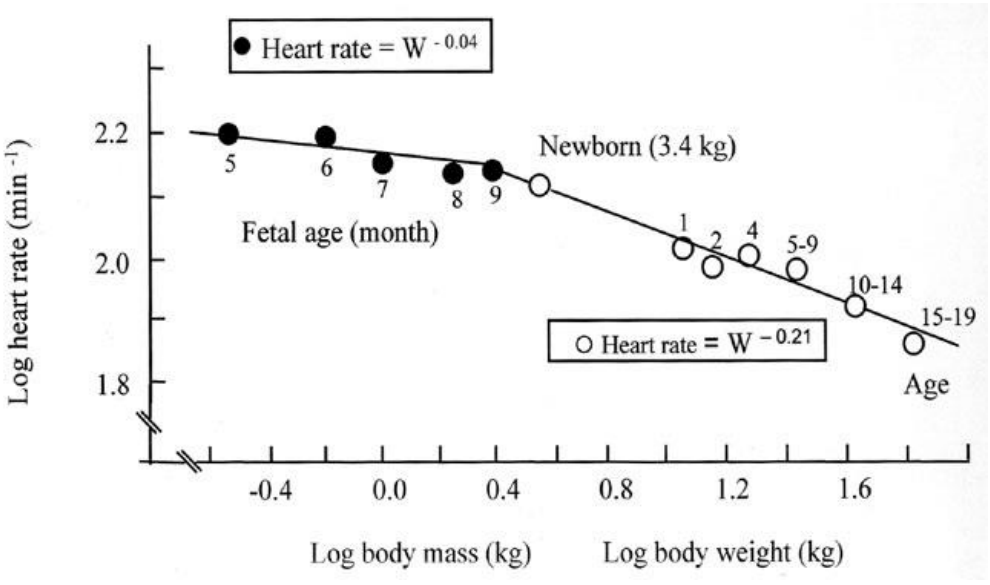

Figure 6. Double logarithmic plot of heart rate (beats min-1) as function of body weight in the fetal (filled symbols) and postnatal life (open symbols). Data are from Altman & Dittmer (1964).

3. The Heart.

The heart is a muscular organ and it works as a mechanical pump pushing the blood through the vessels in order to diffuse the oxygen and nutrients in the whole body. In mammals, the heart is organized into four chambers: right and left atria, right and left ventricles. Due to the presence of atrioventricular valves (tricuspid and mitral –bicuspid-), the circulation is allowed only from the atria to the ventricles avoiding the blood reflux to the lungs. To synchronize the process, the blood pumping is set with a precise contraction sequence. For this reason, in the heart it is possible to classify muscle cells into **working myocardium** or **conduction system**.

I. The Working Myocardium.

In the working myocardium, cardiomyocytes build the atria and the ventricles and through their contraction generate the tension necessary to circulate the blood. Every cardiomyocyte is electrically coupled to the next through low-resistant gap junctions (connexins) so that the heart can be considered as a *functional syncytium*.

II. The Conduction System

While in the skeletal muscle, the electrical impulse that trigger the contraction origins in the nervous system, in the heart the signal, in the form of spontaneous and repetitive action potentials, is generated from specialized cells of the conduction system. . These cells represent the pacemaker regions of the heart. Due to their role, these pacemaker cells have rudimentary contractile filaments and indeed, they contract relatively weakly if compared

with cells of the working myocardium. Sinoatrial cells, for example, are generally smaller, do not show striations and have a peculiar spindle shape. (DiFrancesco et al., 1986)

In the heart, there are several pacemakers (see Figure 7A):

- the sinoatrial node (SAN)
- the atrioventricular node (AVN)
- His bundle (His)

Physiologically, the main pacemaker of the heart is the sinoatrial node (sinus node, SAN) located in the wall of the right atrium near the entrance of superior vena cava. SAN cardiomyocytes form the "*natural pacemaker*" of the heart". The reason why SAN acts as the main pacemaker region is that SAN cells, due to a unique combination of ion currents (Figure 7B), generate action potentials with a higher rate than the other pacemaker regions in phenomena called "*overdrive suppression*". The functional architecture of the SAN tissue includes a central part near the sinoatrial artery ("*primary pacemaker cells*") surrounded by peripheral cells ("*secondary pacemaker cells*"). Both primary and secondary pacemaker cells spontaneously fire, but in physiological conditions, only the primary pacemaker cells generate the electrical impulse (Dobrzynski et al., 2013). Secondary pacemaker cells have different roles:

1. protecting the primary pacemaker cells from the influence of atrial cardiomyocytes;
2. helping the correct propagation of the electrical stimulus;
3. becoming the leading pacemaker when some problems occur in the SAN (Dobrzynski et al., 2013).

The electrical impulse originated by the SAN travels rapidly across the atria and then, slows down in the AVN in order to let the atria contraction to finish before ventricles start to contract. AVN works as a “back-up” pacemaker in case of SAN failure. At this point, the stimulus reaches the His bundle that depart from the AVN and then it rapidly spreads through Purkinje fibers in the ventricles.

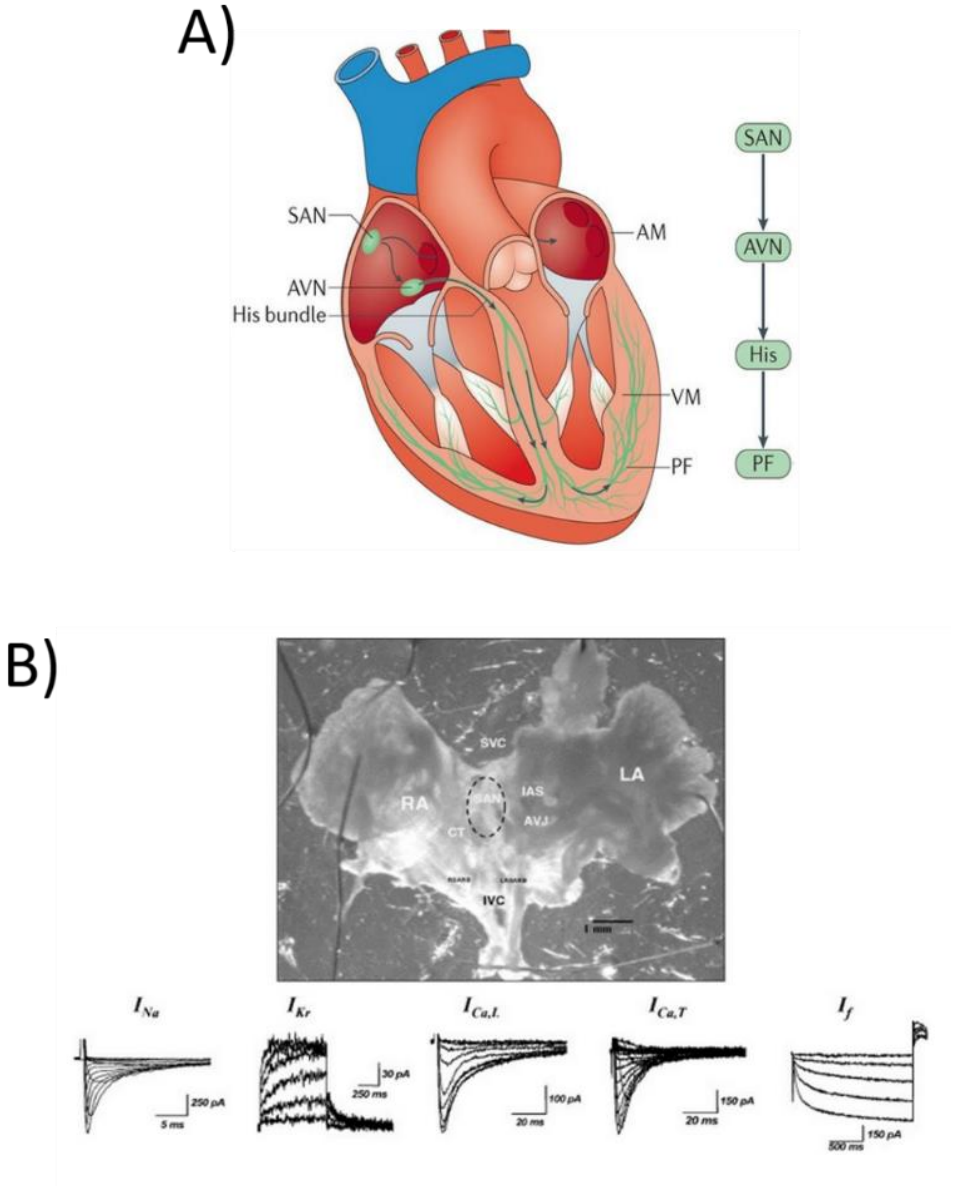

Figure 7. A) Schematic representation of the cardiac conduction system. Sinus node (SAN), Atrioventricular Node (AVN), His Bundle (His), Purkinjie Fibers (PF), Atrial Myocardium (AM), Ventricular Myocardium (VM). From Cingolani et al., 2018. B) Mouse SAN tissue limited by crista terminalis (CT) and by the superior and inferior cavae veins (SVC, IVC) which are cut along their major axis. (RA) and (LA) indicate the right and left atrium, respectively, separated by the interatrial septum (IAS). On the bottom, representative traces of ion currents recorded in SAN cells. From Mangoni et al., 2006.

The autonomic nervous system physiologically participates to the activity of the heart because of the presence of sympathetic (SNS) and parasympathetic (PSNS) branches in cardiac tissue. Release of catecholamines that bind to β-receptors in cardiac tissues cause an increase of: - the contraction force of the fiber (positive *inotropy*); - the AVN conduction velocity (positive *dromotropy*); - the heart rate (positive *chronotropy*); - the electrical excitability (positive *bathmotropy*). Instead, PSNS has opposite effects in the heart due to the release of acetylcholine that bind to the muscarinic receptors in the heart.

In humans, PSNS influences the heart physiology more than the SNS resulting in a resting adult heart rate in a range between 60 and 100 bpm. Anomalies of the heart rate (**arrhythmias**) can result in bradycardia (<60 bpm at rest) or tachycardia (>100 bpm at rest). There are four main types of cardiac arrhythmias:

- *Premature heart beats* (extra beats): the most common arrhythmia. Premature atrial, ventricular or junctional contractions happen during life and they can be associated with stress, caffeine or smoking. They generally do not need any pharmacological treatment or have long-term complications.
- *Supraventricular tachycardia (SVT):* is a fast heart rate condition that originates in the upper part of heart due to the presence of re-entry circuits or an increased cardiac automaticity. It includes atrial fibrillation, paroxysmal supraventricular tachycardia, atrial flutter and the Wolff-Parkinson-White syndrome.
- *Ventricular arrhythmias*: occur in the lower part of the heart. They include ventricular tachycardia (in which the SAN loses the control of heart rate and the electrical stimulus originates in secondary

pacemakers) and ventricular fibrillation (several impulses originates from different areas resulting in a not-controlled fast heartbeat that does not allow a proper blood circulation).

- *Bradyarrhythmias*: is a slow heart rate that can be related to: - a structural adaptation (as the hypertrophic heart of an athlete); - a change in vagal tone; - a dysfunction in the SAN (*Sick Sinus Syndrome)*; - anomalies in the conduction system efficiency.

4. The Cardiac Action Potential.

Action potential is a fast change in cellular membrane potential that is caused by an exchange of ions across the cellular membrane. Cardiomyocytes are electrically excitable cells and they can produce different action potentials (APs) due to a differential expression of ion channels on the cellular membrane. It is possible to distinguish five different phases in a typical model of ventricular AP (Fig. 8):

- ***Phase 0***: consists in a fast depolarization of the membrane potential from -90 mV (resting membrane potential, RMP) to +50 mV due to the activation of sodium channels (I_{Na}). Sodium channels activate when the electrical stimulus causes the depolarization of the RMP to ≈-65 mV (threshold value). Only if the threshold is reached, the action potential can originate. AP is a "*all or none*" phenomenon. In SAN cells, the opening of L-type ("*long lasting*") calcium channels (I_{CaL}) causes the depolarization during the phase 0. These channels activate slower than sodium channels as demonstrated by a reduced value of the slope that represents the maximum rate of voltage change (dV/dT_{max}). Moreover, phase 0 lasts less than 2ms in ventricular myocytes while it is slower in SAN cells (10/20 ms).
- ***Phase 1***: after the AP reaches the depolarization peak in phase 0, there is a transient repolarization of the membrane potential due to a simultaneous inactivation of sodium channels and activation of the "*transient outward*" potassium current (I_{to}). Physiologically, the inactivation of sodium channels guarantees the *absolute refractory period* in which the cardiomyocytes cannot produce a new action potential. Indeed, sodium channels recover from inactivation when the membrane hyperpolarizes and then, they move on the closed

conformation. It is not possible to pass directly from the inactivated to the open conformation; the channels must close before re-activating and ensuring the refractoriness. During phase 1, the membrane potential does not complete the repolarization to RMP due to the rapid inactivation of I_{to} potassium channels.

- ***Phase 2***: also referred as the "*plateau phase*" in which an electrical balance between inward calcium (I_{CaT} and I_{CaL}) currents and outward potassium currents (delayed rectifier potassium channels) is established. During phase 2, calcium ions enter inside the cell and bind the ryanodine receptors (RYR) on the sarcoplasmic reticulum (SR) allowing the calcium flow in the cytosol ("*Calcium-induced calcium release"*) a mechanism known as excitation-contraction coupling. Considering that contraction in the working myocardium is fundamental, it is understandable the reason why SANCs completely lacks this phase.
- ***Phase 3:*** consists in the rapid repolarization of the AP. In this phase, L-type calcium channels inactivate, while slow delayed rectifier (I_{Ks}) potassium channels (activated during phase 2) remain open allowing a net outward positive current. During the repolarization, other potassium channels open: *rapid delayed rectifier* (I_{Kr}) and *inwardly rectifying* (I_{K1}) channels. I_{Kr} channels close in proximity of RMP while I_{K1} remains active throughout the phase 4 setting the RMP. In the SAN, phase 3 depends on the inactivation of L-type calcium channels and the opening of I_{Kr} channels. During phase 3, there is the "*relative refractory period*", in which due to the more hyperpolarized potential, sodium channels partially recover from the inactivation passing to the closed conformation. In this period, it is possible to evoke a new AP

only with a stronger stimulus that allows the complete activation of sodium channels.

- ***Phase 4:*** in non-pacemaker cells, it occurs when the cell reaches the resting potential around -90mV (diastole phase). Ion concentration is continuously restored by the activity of ion pumps that guarantee the physiological ion concentrations inside and outside the cell. Physiologically RMP results from I_{K1}. In the pacemaker cells, there is not a RMP; when the cell reaches -70 mV, a slow depolarization occurs (diastolic depolarization) due to the activation of HCN channels (I_f current). During the second part of the diastolic depolarization, T-type ("Transient") calcium channels activate causing the crossing the threshold to evoke a new AP.

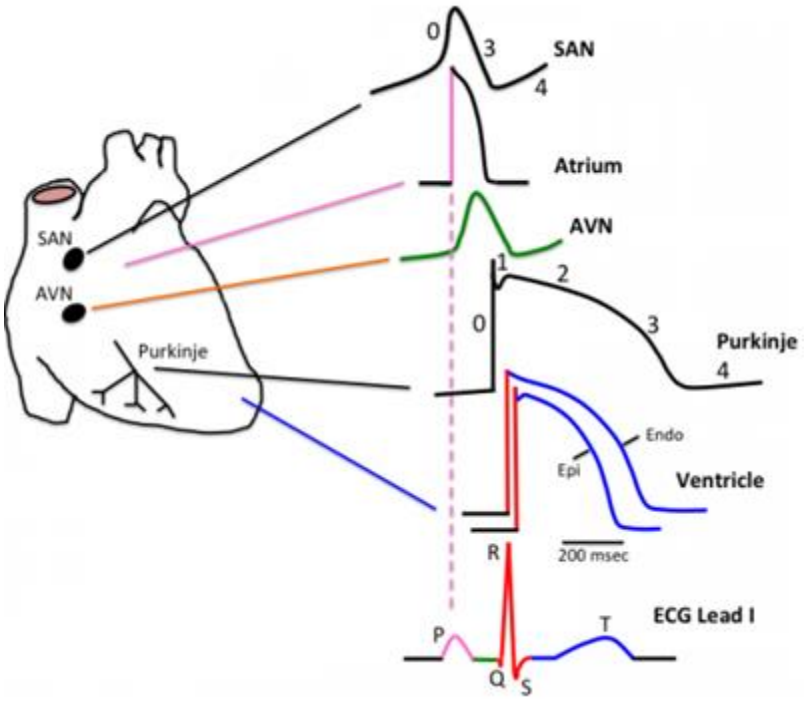

Figure 8. Schematic representation of Action Potentials in different regions of the heart. On the bottom, a schematic representation of a human ECG to show the correlation between action potentials and cardiac cycle. Adapted from Hume et al., 2012

5. HCN Channels.

Hyperpolarization-activated Cyclic Nucleotide-gated (HCN) channel family consist of four isoforms: HCN1, HCN2, HCN3 and HCN4. HCN1, HCN2 and HCN4 have been reported in both heart and brain tissues, while HCN3 seems to be confined in neurons (Moosmang et al., 2001). HCN4 is the main isoform expressed in the SAN in all species tested (human, mouse, rabbit) (Chandler et al., 2009, Brioschi et al., 2009). While HCN2 is the most abundant isoform in ventricles, HCN1 is also expressed in the SAN and the atria (Herrmann et al., 2011). Based on the homology in sequence, HCN channels can be considered as members of the voltage-gated potassium Kv channels superfamily and of CNG cyclic nucleotide-gated channels (Ulens e Siegelbaum, 2003, Santoro et al., 1997). These channels work as a tetramer in which each subunit is composed of six different transmembrane helical domains (S1-S6). (Zagotta et al., 2003). The core of HCN channels is well conserved (>80%) among the isoforms while N-terminus and C-terminus are more divergent. Structurally, HCN channels have:

1. a voltage sensor localized in the positively charged S4 domain;
2. the GYG pore (between S5 and S6) sequence typical of potassium channels;
3. the CNBD domain that is able to bind cyclic nucleotides in the C-terminus (Baruscotti et al., 2005) (see Figure 9).

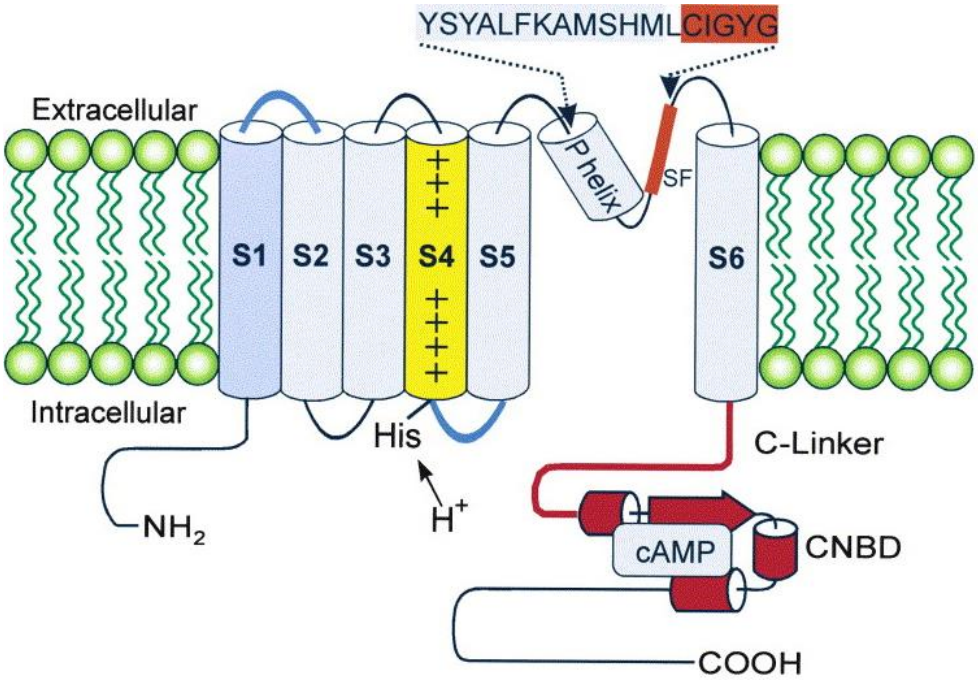

Figure 9. Structural representation of HCN channel subunit. From Biel et al.,2002.

As mentioned before, HCN channels are the molecular components for a hyperpolarization-activated current ("funny current", I_f) that sustains the slow diastolic depolarization in pacemaker cells. A similar current, I_h, has also been described in neurons where it contributes to the AP firing, excitability and modulation of synaptic activity (Pape et al., 1996, Robinson et al., 2003). I_f has a "*funny*" behaviour: it activates upon membrane hyperpolarization, it is activated both by voltage and cyclic nucleotides (Figure 10A). The activation gate of HCN channels is closed when the S4 is in its outermost configuration at positive voltages but open in other channels. This "inverted" gating model is supported by a recent study indicating that the S4–S5 linker of HCN channels couples the movement of the voltage-sensing S4 helix to the opening and closing of the gate as previously proposed for depolarization-activated potassium channels (Chen et al. 2001).

The primary sequence of the pore contains the same glycine-tyrosine-glycine (GYG) motif of highly selective K^+ channels. Curiously, HCN channels are not selective for K^+ ions but they allow other monovalent ions to permeate including Na^+ and K^+ with a relative permeability ratio P_{Na+}/P_{K+} of 0.20 (Gauss et al. 1998, Ludwig et al. 1998, Santoro et al. 1998). Under physiological conditions HCN channels mediate an inward Na^+ current and not a K^+ current. In tetrameric K^+ channels, four copies of GYG motifs provide the selectivity filter for K^+ ions (Lu et al. 2001, Zhou et al. 2001). The presence of a single GYG sequence in HCN channels indicates that one copy of this motif is not sufficient to confer selectivity for K+ ions. This could be explained by a different spatial configuration of the channel due to a change in the protein folding.

When overexpressed in heterologous systems, all the HCN isoforms either alone or in combination failed to reproduce completely the native I_f suggesting that cellular environment is essential to modulate its properties (Altomare et al., 2003, Qu et al., 2002). From its first discovery in rabbit SANCs in late 1970s (Brown et al., 1979), I_f current was found not only in the primary pacemaker of other species, like human (Verkerk et al., 2007) and mouse (Mangoni et al., 2001) but also in several regions of the conduction system including the AVN (Choisy et al., 2015) and Purkinjie fibers (DiFrancesco, 1981). However, its detection seems to be restricted not only in pacemaker cardiomyocytes and in embryonic/new born ventricular myocytes (Robinson et al., 1997, Wang et al., 2013) where they contribute to the generation of action potentials (Figure 10B). Recent studies have demonstrated that f-channels are also present in non-pacemaker cardiomyocytes, and become upregulated in cardiac hypertrophy and failure where they may contribute to the generation of an arrhythmogenic substrate (Cerbai & Mugelli, 2006).

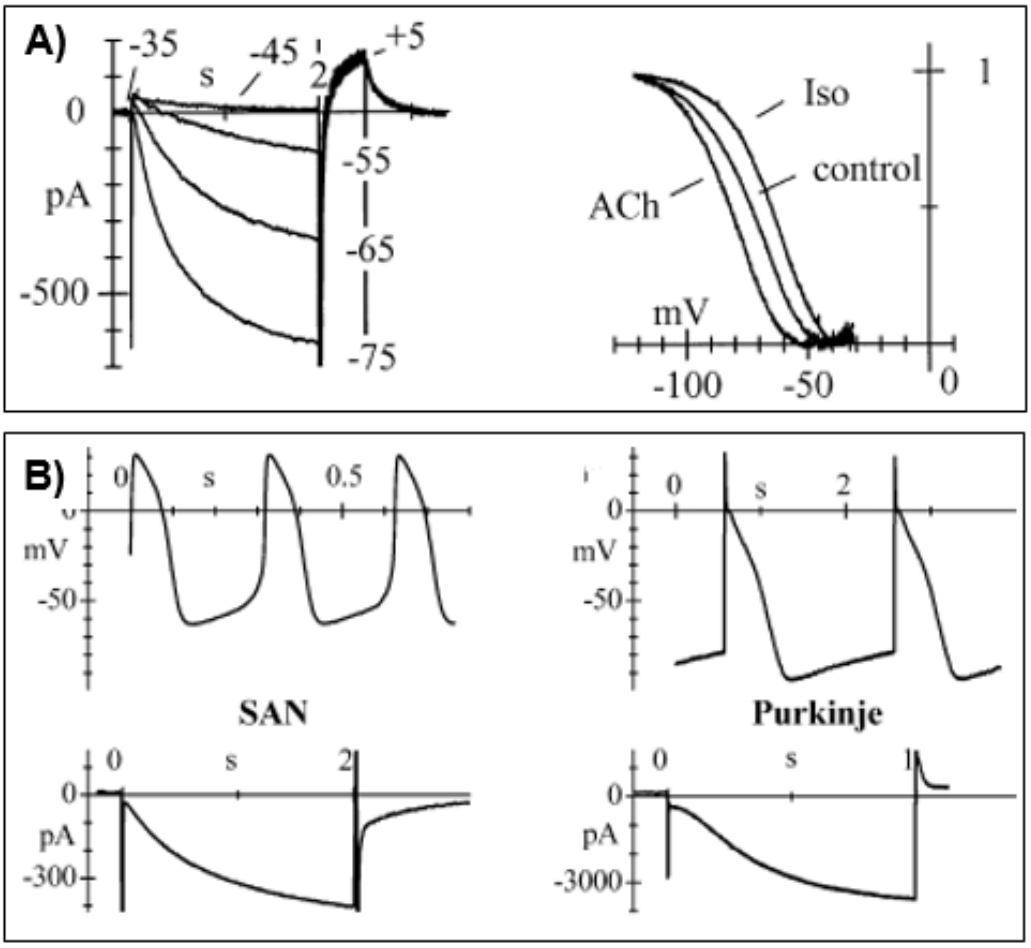

Figure 10. A) I_f current traces recorded in SAN myocyte during steps to the voltages as indicated. On the right, the effect of adrenergic (Iso) and muscarinic (ACh) stimulation on the activation curve of I_f. Adapted from Baruscotti et al., 2004. B) Comparison of I_f current and the generation of action potentials between SAN and Purkinje cells. Adapted from Barbuti et al., 2007.

The I_f is not the only current sustaining the diastolic depolarization since it has been demonstrated that spontaneous beating activity does not stop in presence of caesium, an I_f blocker (Denyer et al.,1990). On the other hand, Ivabradine (Servier) inhibits selectively HCN channels causing a reduction of heart rate without side effects. Ivabradine causes the slowing of the firing rate of SAN myocytes reducing the slope of the diastolic depolarization

phase (Bucchi et al., 2006) suggesting a central role of this current in setting cardiac rate. Spontaneously beating mouse SAN cells that show an intrinsic fast action potential rate due to a high *in vivo* heart rate, display a greater I_f current density (Baruscotti et al., 2011). Furthermore, a transgenic mouse model with an inducible-cardiac specific *Hcn4* KO causes *in vivo* deep bradycardia suggesting a correlation between HCN channels and heart rate (Baruscotti et al., 2011).

6. L-type Calcium Channels.

The L-type Calcium channels (LTCCs) belongs to the voltage-dependent calcium channels (VDCCs) family together with T-, P-, N- and R-type calcium channels. "L" stands for "*long lasting*" referring to their relatively long duration of activation. Structurally, they have a pore-forming subunit (α1) that is organized into four homologous domains (I-IV). Each domain consists of the six α-helical transmembrane domains that present:

1. the voltage sensor localized in S4 region;
2. a P-loop constituting selectivity filter of;
3. the channel pore resulting from S6 segments association (Figure 11) (Striessnig et al., 1999).

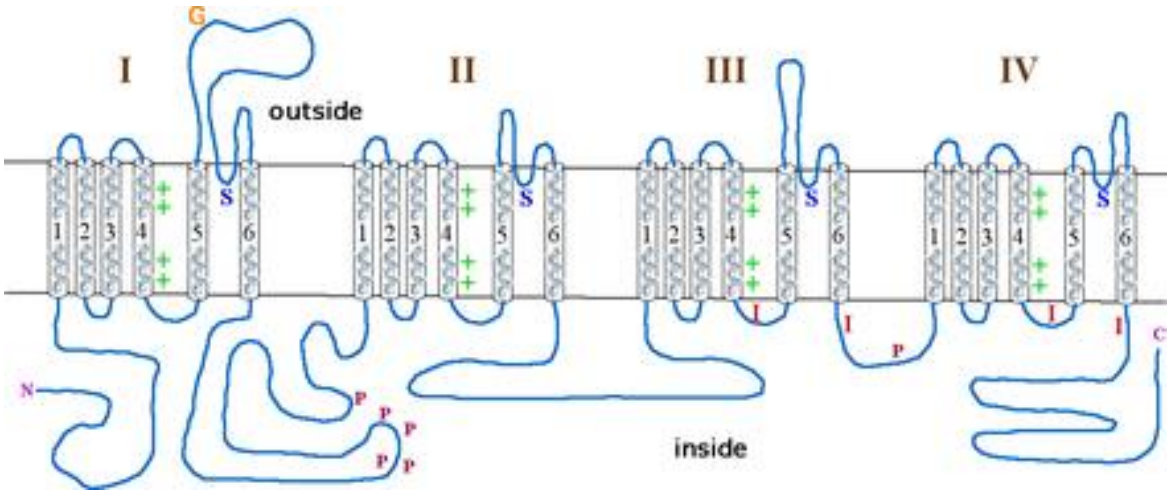

Figure 11. Schematic representation of α_1 subunit.

α_1 subunit associates with auxiliary subunits (β, α2δ and γ) and calmodulin to assemble the fully functional channel. Based on the different α1 subunits, LTCCs are indicated as CAV1.1, CAV1.2, CAV1.3 or CAV1.4 (as shown

in Table 1) and they are all sensitive to dihydropyridines (DHPs) with differences in affinity.

α1 GENE NAME	**PROTEIN NAME**
Cacna1s	CAV1.1
Cacna1c	CAV1.2
Cacna1d	CAV1.3
Cacna1f	CAV1.4

Table 1. Gene names encoding for L-type calcium channels.

LTCCs are expressed throughout the body with a specific organization in the tissues. CAV1.1 is the main isoform of the skeletal muscle where it mediates the excitation-contraction (EC) coupling (Tanabe et al., 1988); CAV1.4 is mainly expressed in the immunity system (Kotturi et al., 2003), spinal cord and retina (McRory et al., 2004). CAV1.2 and CAV1.3 are present in the brain, endocrine cells and in the heart (Catteral et al., 2000). In the endocrine cells, LTCCs mediate both the aldosterone secretion in the adrenal cortex (Barrett et al., 2016) and the endocytosis of catecholamines from chromaffin cells (Rosa et al., 2012). In the heart, CAV1.2 is the most abundant LTCC isoform and it is essential in the EC coupling in the working myocardium. CAV1.2 is generally considered the main determinant of I_{CaL} in the heart. Indeed, CAV1.3 was thought to be present specifically in neurons (Hell et al., 1993), only recently it has been demonstrated that is present in the atria and in the SAN (Mangoni et al., 2003). CAV1.3 show less sensitivity for DHPs (Xu et al., 2001), a lower voltage threshold for activation (-50 mV)

(see Figure 12) and slower inactivation kinetics than CAV1.2 channels (Koschak et al., 2001).

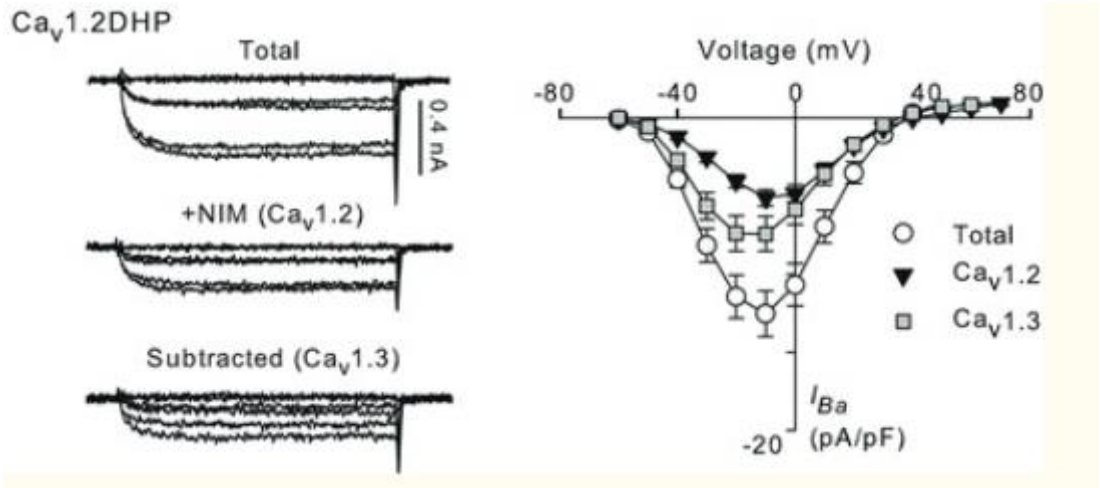

Figure 12. Representative traces and current-voltage curves of the mean current density of total CAV1.2+CAV1.3 current, CAV1.2 current and CAV1.3 current in murine sinoatrial cells. Adapted from Christel et al., 2012.

In addition to the "*membrane clock*" model of pacemaker activity in the heart which considers I_f as the starter of the diastolic depolarization, the "*calcium clock*" model indicates that spontaneous rhythmic Ca^{2+} release from the SR activates the Na^+/Ca^{2+} exchanger (NCX) mediating a net inward current that is able to depolarize the membrane voltage to the threshold (Bogdanov et al., 2001). Recently, this model has been updated into the "*coupled-clock*" model, adding the membrane calcium channels involvement to generate the pacemaker activity (Lakatta et al., 2010). Indeed, Ca^{2+} channels can be found in isolated rabbit SAN cells where they can influence the cellular beating rate (Hagiwara et al., 1988). Moreover, the administration of Nifedipine (a specific LTCC blocker) blocks the automaticity in the centre of rabbit SAN

but not in its periphery (Kodama et al., 1997). CAV1.2 and CAV1.3 are both involved in the pacemaker activity, with an emerging role of CAV1.3 into the diastolic depolarization phase (Mangoni et al., 2003). Indeed, the evidence that CAV1.3 activates more rapidly and at more negative potentials, suggests that CAV1.3 to contribute more significantly than CAV1.2 to the slow diastolic depolarization phase. To dissect CAV1.2 and CAV1.3 contributions to the SAN automaticity, a transgenic mouse model in which CAV1.2 is insensitive to DHPs was generated (Sinnegger-Brauns et al., 2004, Christel et al., 2012). Christel and colleagues demonstrated not only a major contribution of CAV1.3 to the diastolic depolarization but also the evidence that only CAV1.3 channels are strongly co-localized with RYR2 in the SAN cells. This co-localization facilitates the RYR-mediated calcium release during the late diastolic depolarization. As shown in figure 13, the transgenic mouse model of *Cacna1d* KO ($CAV1.3^{-/-}$) displays bradycardia associated with sinoatrial arrhythmia (Platzer et al., 2000). This phenotype is independent by the system nervous system as demonstrated by the evidence that isolated $CAV1.3^{-/-}$ SAN cells show a lower and irregular action potentials firing rate *in vitro* when compared with WT cells (Mangoni et al., 2003).

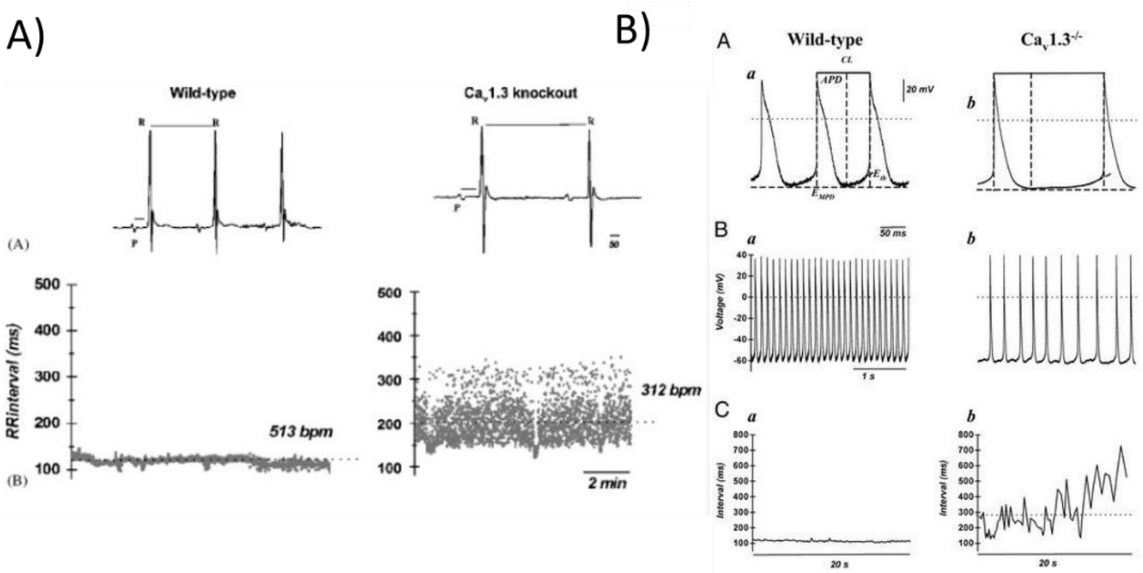

Figure 13. A) ECGs recorded from freely moving WT and CAV1.3$^{-/-}$ mice. B) Recorded spontaneous action potentials from WT and CAV1.3$^{-/-}$ SAN cells. On the bottom, analysis of AP interval between WT and CAV1.3$^{-/-}$ cells. From Mangoni et al., 2006.

LTCCs can be also modulated by the activity of the autonomic nervous system in both a positive and negative way. β-adrenergic stimulation leads to the production of cyclic-adenosine-monophosphate (cAMP) that is necessary to activate PKA. While it has been demonstrated that cAMP can directly activate f-channels binding their CNBD domain (DiFrancesco et al., 1991), the PKA-dependent phosphorylation increase LTCC conductance (Mangoni et al., 2003).

Aim

The transcription factor NFIX is expressed in several tissues and it is important both during development and in adulthood. It has a pivotal role in the skeletal muscle modulating not only transcriptional switch from embryonic to fetal myogenesis but also the regeneration process in the adult mice (Messina et al., 2010, Rossi et al., 2016). Until now, the expression profile and the role of NFIX in the heart has never been studied. Since skeletal and cardiac muscle share several physiological properties, the aim of my PhD thesis was to investigate for the first time the role of this transcription factor in heart function. To reach this purpose I will perform *in vivo* experiments in *Nfix*-deficient mice and age-matched WT controls to investigate the phenotype of NFIX loss-of-function. I will also use RNA interference to downregulate *Nfix*-transcript in an *in vitro* model of rat neonatal cardiomyocytes to perform electrophysiological experiments.

Materials and methods

1. Statistical Analysis

All the data are displayed as Mean Value ± Standard Error of the Mean. Either Student's T-test or One-Way ANOVA (followed by Fisher's Low Standard Deviation post-hoc test) were used to determine if there are differences between two (T-test) or more (ANOVA) independent data sets (*$p \leq 0.05$). Shapiro-Wilk normality test was performed on each data set and at the 0.05 level, they confirmed a normal distributed population.

2. Mouse model

This project has been developed in collaboration with the group of prof. Graziella Messina who gave us the possibility to use *Nfix*-null mice (C57 BL6/1295) and wild type (WT) littermates or age-matched mice as controls. *Nfix*-null mice were generated crossing heterozygous *Nfix*-null$^{+/-}$ mice obtained from Prof. Richard M. Gronostajski of University of Buffalo. Due to the severe phenotype of *Nfix*-null, from postnatal day 21, the food was supplemented with a soft dough chow (*Transgenic Dough Diet, Bioserv*), as previously described (Campbell et al., 2008). All the procedures were conformed to Italian law (D. Lgs n° 2014/26, implementation of the 2010/63/UE) and approved by the Università degli Studi di Milano and its Animal Welfare Body (OPBA) and the Italian Minister of Health (n.273/2018-PR).

3. RNA Extraction and Retrotranscription

To isolate RNA from tissues, *RNAse*-free glass mortar tubes, pestles, and sterile insulin needles were used to homogenize the sample in 1 mL of TRIzol® Reagent (*Thermo Fisher*). After the mechanical disruption of cell membrane, the sample was centrifuged at 12'000 g x 5 minutes and the supernatant was transferred in a new *RNAse*-free tube. At this point, 200 µL of Chloroform:Isoamyl alcohol 49:1 (*Sigma Aldrich*) was added to the mixture, inverted and then incubate for 4 minutes at room temperature. The sample was centrifuged at 12'000 g x 15 minutes at 4-10°C. After the centrifuge, it is possible to recognize three different density phases in the sample:

- An aqueous phase containing RNA;
- An intermediate phase;
- An organic phase containing DNA and proteins.

Only the aqueous phase is transferred in a new RNAse-free tube in which 1 µL of 20 µg/mL Glycogen (*Thermo Fisher*) and 400 µL of Isopropanol (*Sigma Aldrich*) were added and gently inverted ten times. To facilitate RNA precipitation, the sample was incubated for 10 minutes at room temperature and then centrifuged at 12'000 g x 10 min at 4-10°C. RNA pellet was washed for three times in 1 mL of cold 75% Ethanol (*Sigma Aldrich*) and centrifuged at 7'500 g x 5 min at 4-10°C. After discarding the supernatant and the complete evaporation of ethanol from the tube, the pellet was risuspended in MilliQ Water (*Millipore-Sigma Aldrich*) and incubated for 10 minutes at 60°C. Fresh isolated RNA was then stored at –80°C. RNA was quantified using Ultrospec® 500/1100 pro spectrophotometer (*Amersham Biosciences*) and proteins and phenols contamination were evaluated using ABS_{260nm}/ABS_{280nm} and ABS_{260nm}/ABS_{230nm} values. To eliminate residual

genomic DNA, 1 µg of total RNA from each sample was treated with *DNAse I RNAse-Free* (*Thermo Scientific*) using the mixture in Table 1 and incubated for 30 minutes at 37°C. To block DNAse I activity, 1 µL of 50mM EDTA was added to the mixture and then incubate it for 10 minutes at 65°C. cDNA retrotranscription with random examers of DNAse-treated RNA was performed using *Thermo Fisher*'s Kit "*cDNA Synthesis Kit for RT-qPCR*" (Table 2) following different temperature steps: 25°C for 10 minutes, 50°C for 15 minutes and 85°C for 5 minutes.

	Quantity
RNA	1 µg
DNAse I 1U/µL	1 µL
Buffer $MgCl_2$ 10X	1 µL
Milli-Q® Water	Up to the volume
Final Volume	10 µL

Table 1 DNAse I mixture.

	Quantity
DNAse-treated RNA	1 µg
Buffer Reaction Mix 5X	4 µL
Maxime Enzyme Mix 10X	2 µL
Milli-Q® Water	Up to the volume
Final Volume	20 µL

Table 2 Retrotranscription mixture.

4. qPCR and RNA sequencing

Gene expression was quantified by real-time qPCR (Line-gene 9600plus, Bioer); experiments were carried out using *Maxima SYBR Green/ROX qPCR Master Mix* (*Thermo Scientific*) as shown in Tables 3 and 4. qPCR conditions were: first step at 95°C for 5 minutes followed by 45 cycles at 95°C for 15 seconds, 60°C for 30 seconds and 72°C for 30 seconds. The melting curve analysis (60°C to 96°C) was performed at the end of the protocol to verify the presence of a single amplicon. Each sample was run in triplicate and the mean cycle threshold (Ct) of the gene of interest (GOI) was normalized to the mean Ct of the housekeeping (HSK) gene (*Gapdh* or *Rps15a*). The data are displayed as $2^{-\Delta Ct}$*100±SEM, considering $\Delta Ct=Ct_{GOI}-Ct_{HSK}$. The data are displayed as $2^{-\Delta Ct}$*100±SEM, considering $\Delta Ct=Ct_{GOI}-Ct_{HSK}$. Because of the large range of values among the populations, statistical analysis was performed with the logarithm $2^{-\Delta Ct}$*100 as used in literature (Scavone et al., 2013).

	Quantity
cDNA	10 ng
Forward Primer 10 μM*	1.25 μL
Reverse Primer 10 μM*	1.25 μL
SYBR® 2X	12.5 μL
Milli-Q® Water	Up to the volume
Final Volume	25 μL

Table 3 Real-time qPCR mixture.

GENE NAME	FORWARD PRIMER 5'→3'	REVERSE PRIMER 5'→3'
Mus musculus *Nfix*	CTGGCTTACTTTGTCCACACT	CCAGCTCTGTCACATTCCAGA
Mus musculus *Gapdh*	AGGTCGGTGTGAACGGATTTG	TGTAGACCATGTAGTTGAGGTCA
Mus musculus *Rps15a*	AAACTGACGTGAAGGGAGCA	CCTCACAGGAAGGTTGAACAAG
Mus musculus *Nkx2.5*	GACGTAGCCTGGTGTCTCG	GTGTGGAATCCGTCGAAAGT
Mus musculus *Myh6*	TGCTCAGAGCTCAAGAAGGAT	CCCAGCCATCTCCTCTGTTA
Mus musculus *Myh7*	CAGCAGACTCTGGAGGCTCTT	AGGGCGACCTCAACGAGAT
Mus musculus *Mlc2v*	GGACACATTTGCTGCCCTA	ATCGTGAGGAACACGGTGA
Mus musculus *Cacna1c*	TAGTGTCCGGAGTCCCAAGT	GAAGAGCACAAGAAGGGCAAT
Mus musculus *Cacna1d*	GTTGTAAGTGCGGTAGAAAGCA	CTGGTGCCTCTTGCATAGTTT

Mus musculus *Cacna1g*	TAACCTGCTTGTCGCCATT	ACTCGTATCTTCCCGTTTGC
Mus musculus *Cacna1h*	CCTGCTGGACACTGTGGTT	GGAGCATGAAAAGAAGACCAA
Rattus norvegicus *Nfix*	CTGGCTTACTTTGTCCACACT	CCAGCTCTGTCACGTTCCAGAC
Rattus norvegicus G*apdh*	GATTTGGCCGTATCGGAC	GAAGACGCCAGTAGACTC

Table 4 Primers sequences. All primer pairs were tested for an efficiency >95%.

5. Histological Analysis

Hearts were blocked in diastole using 100 nM $CdCl_2$ (*Sigma Aldrich*) and immediately fixed in 4% PFA (*Sigma Aldrich*). Excess of fixative was removed with two washes with PBS (*Sigma Aldrich*) of 5 minutes each under gentle shaking. Samples were successively re-equilibrated in PBS-sucrose solutions at increasing sucrose concentrations: 1h with 7,5% sucrose, 1h with 15% sucrose, and O/N in 30% sucrose, at 4°C under constant shaking. The day after, samples were embedded in OCT (*Bio-Optica*), included in nitrogen-cooled isopentane (*VWR*), and maintained at -80°C until further processing. For Hematoxilin and Eosin and Milligan's Trichrome stainings, 7µm sections were cut with a cryostat (*Leica*) on positively charged glass slides (*Superfrost Plus, Thermo Scientific*). Muscle sections were stained with hematoxylin and eosin (*Sigma Aldrich*) according to standard protocols. Briefly, samples were washed in distilled water and stained with hematoxylin for 4 minutes. Excess of staining was removed with a 15 minutes wash under running water, then slices were progressively dehydrated to 90% Ethanol (*VWR*) and stained for 7 minutes with 0,5% Eosin in 90% Ethanol. Slices were then further dehydrated through successive steps in graded alcohol solutions, cleared with xylene (*VWR*) and mounted with Eukitt mounting medium (*Bio-Optica*). For Milligan's trichrome, sections were fixed for 1 hour with Bouin's fixative (*Sigma Aldrich*) and rinsed for 1 hour under running water. Sections were then rapidly dehydrated to 95% Ethanol in graded ethanol solutions; successively they were passed in 3% potassium dichromate (*Sigma Aldrich*) for 5 minutes and rapidly washed in distilled water. Then, they were stained with 0,1% acid fuchsin (*Sigma Aldrich*) for 30 seconds, washed again in distilled water and passed in 1% phosphomolybdic acid (*Sigma Aldrich*) for 3 minutes.

After, they were stained with Orange G (2% in 1% phosphomolybdic acid) (*Sigma Aldrich*) for 5 minutes, rinsed in distilled water, passed in 1% acetic acid (VWR) for 2 minutes, stained with 1% Fast Green for 5min (Sigma-Aldrich), passed in 1% acetic acid for 3 minutes, rapidly dehydrated to 100% Ethanol and cleared in Xylene before mounting with Eukitt (*Bio-Optica*). Images were acquired with a *Leica-DMI6000B* microscope equipped with a 10X magnification objective. Leica DFC400 camera was used for image capture.

6. In vivo Telemetry

6 month-old male mice were implanted with a radio frequency transmitter (*TA10ETA-F20, DSI*) as previously described (Baruscotti et al., 2011). The radio-transmitter allowed the simultaneous recordings of cardiac rate, activity and temperature in freely moving conditions. To allow the complete recovery from the surgery, recordings started 15 days after the surgery. ECGs were collected during both night and day for 5 days giving a 2 minutes recording every 30 minutes. Data were acquired and analyzed with the Dataquest 4.2 software (DSI)..

7. Isolation of Sinoatrial Node Cells (SANCs)

SANCs were isolated from 6-month old *Nfix*-null and WT mice (both males and females). Hearts were explanted and put immediately in Tyrode's solution (mM: 140 NaCl, 5.4 KCl, 1.8 $CaCl_2$, 1 $MgCl_2$, 5.5 D-glucose, 5 Hepes-NaOH; pH 7.4) plus 1000 U Eparin. During the sinus node (SAN) dissection, the tissue is maintained in warm Tyrode and placed onto the stage of a stereoscopic microscope. Once the tissue is dissected, it is cut in 4-5 pieces and immediately washed for three times in a low-calcium solution (mM: NaCl 140, KCl 5.4, $MgCl_2$ 0.5, KH_2PO_4 1.2, HEPES-NaOH 5, Taurine 50, D-Glucose 5.5; pH=6.9) for 1 minute. Then, SAN is enzymatically digested for at least 25 minutes at 37°C using low-calcium solution plus 0.2 mM $CaCl_2$, 1 mg/mL BSA, 0.45 U/mL Protease (*Sigma Aldrich*), 1.30 U/mL Elastase (*Sigma Aldrich*) and 250 U/mL Collagenase IV (*Worthington*). Once the enzymatic incubation is over, SAN is washed three times in zero-calcium solution (mM: KOH 80, L-Glutamic Acid 70, KCl 20, βOH-Butyric Acid 10, KH_2PO_4 10, HEPES-KOH 10, Taurine 10, EGTA-KOH 1; 1 mg/mL BSA, pH=7.4) and then mechanically digested for 10 minutes in 3 mL of zero-calcium solution. Then, cells are gradually adapted to physiological calcium concentrations using the following steps every 4 minutes a 4°C:

1) + 72 µL of a solution containing 10mM NaCl and 1.8 $CaCl_2$;
2) + 153.6 µL of a solution containing 10mM NaCl and 1.8 $CaCl_2$;
3) + 374.4 µL of Tyrode plus 1 mg/mL BSA;
4) + 1200 µL of Tyrode plus 1 mg/mL BSA;
5) + 4200 µL of Tyrode plus 1 mg/mL BSA;

At the end of the protocol, SANCs were plated in the center of 35mm-Petri dishes and maintained at 4°C for the day of the experiment.

8. *Isolation and Infection of neonatal rat ventricular cardiomyocytes (NRVCs)*

Primary cultures of NRVCs were prepared as previously described (Scavone et al., 2013). After 24 hours from NRVCs isolation, 4 µg/mL Polybrene was added to four different plates with 10^6 NRVCs. Two plates were infected with a lentivirus carrying the vector plKO.1 with either a scrambled hairpin sequence (Scramble) or short hairpin RNA specific for downregulating *Nfix*-mRNA (*Nfix*-sh) and puromycin resistance cassette (Figure 1) with a final multiplicity of infection (MOI) of 50.

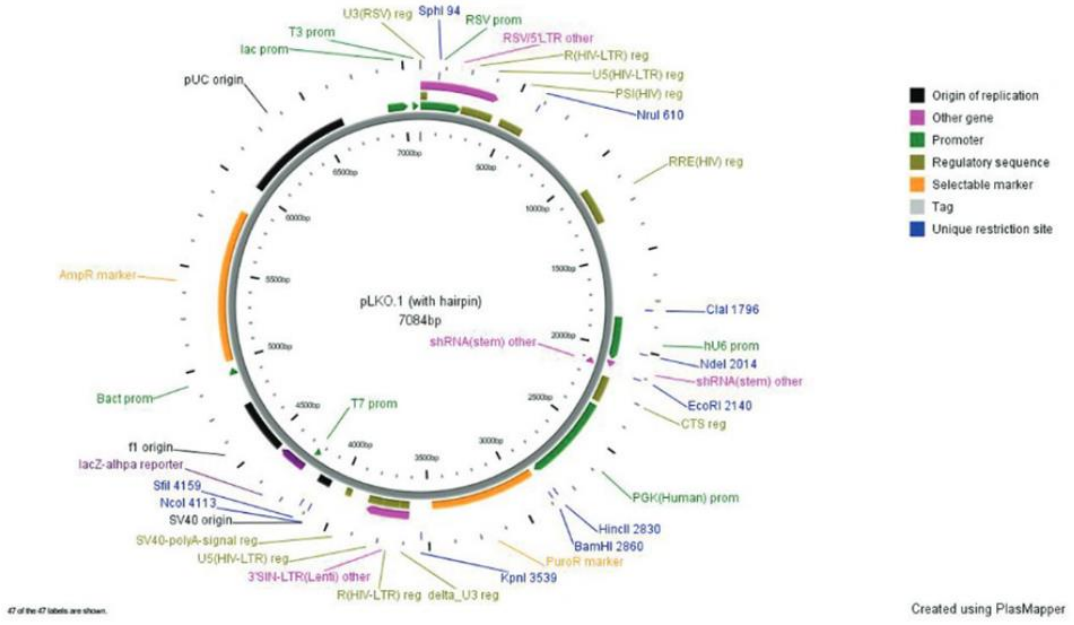

Figure 1. pLKO.1 vector.

After 24 hours from the infection, cells were washed twice in PBS (*Sigma Aldrich*) and Polybrene was removed from all the four plates with NRVCs. Three plates (not infected, Scramble and *Nfix*-sh) were put in stringent 2 µg/mL puromicine selection. After 2 days in puromicine, non-infected NRVCs died, and only the infected cells survived. To evaluate the efficiency of *Nfix* downregulation for each experiment, we compared Nfix expression

level between Not infected NRVCs (that we treated with Polybrene but not with puromicine), Scramble and *Nfix*-sh NRVCs. Two days before single cell electrophysiological recordings, infected NRVCs were dissociated into single cells after incubation for 2-3 minutes with Trypsin-EDTA *(Sigma Aldrich*) a 37°C and centrifuge 300 g for 5 minutes.

9. Electrophysiology

For electrophysiology, cells were placed onto the stage of an inverted microscope and superfused with Tyrode solution containing (mM): 140 NaCl, 5.4 KCl, 1.8 $CaCl_2$, 1 $MgCl_2$, 5.5 D-glucose, 5 Hepes-NaOH; pH 7.4. Patch-clamp pipettes had resistances of 3-6 MΩ when filled with the intracellular-like solution containing (mM): 130 K^+-aspartate, 10 NaCl, 5 EGTA-KOH, 2 $CaCl_2$, 2 $MgCl_2$, 2 ATP (Na^+-salt), 5 creatine phosphate, 0.1 GTP (Na^+-salt), 10 Hepes-KOH; pH 7.2. Temperature was kept at 36±1°C. Spontaneous action potentials were recorded in current-clamp mode using the whole-cell configuration. Action potentials rate, Action Potential Duration at 50% of repolarization phase (APD50), Maximum Diastolic Potential (MDP) and the amplitude of the action potentials were analyzed. For voltage-clamp recordings, only single cells were used. To dissect funny current (I_f) 1 mM $BaCl_2$ and 2 mM $MnCl_2$ were added to Tyrode. Hyperpolarizing test steps to the range -35/ -125 mV (10 mV increments) were applied from a holding potential of -30 mV, followed by a fully activating steps at -125 mV. Each test step was long enough to reach steady-state current activation. Activation curves were obtained from normalized tail currents measured at -125 mV and fitted to the Boltzmann distribution: y= (1/(1+exp((V-V1/2)/s), where V is voltage, y fractional activation, $V_{1/2}$ the half-activation voltage, and s the inverse-slope factor (Figure 2A). For

L-type calcium current (I_{CaL}) recordings, we used a 200 ms voltage ramp protocol from -60 mV to +60 mV (Figure 2B) into an extracellular solution containing (mM): CsCl 10, NaCl 135, $CaCl_2$ 1, $MgCl_2$ 1, HEPES 5, Glucose 11.1, Tetrodotoxin (TTX) 0.03, pH=7.4; To specifically block I_{CaL}, 10µM Nifedipine was added and, then, I_{CaL} was considered as the Nifedipine-sensitive component.

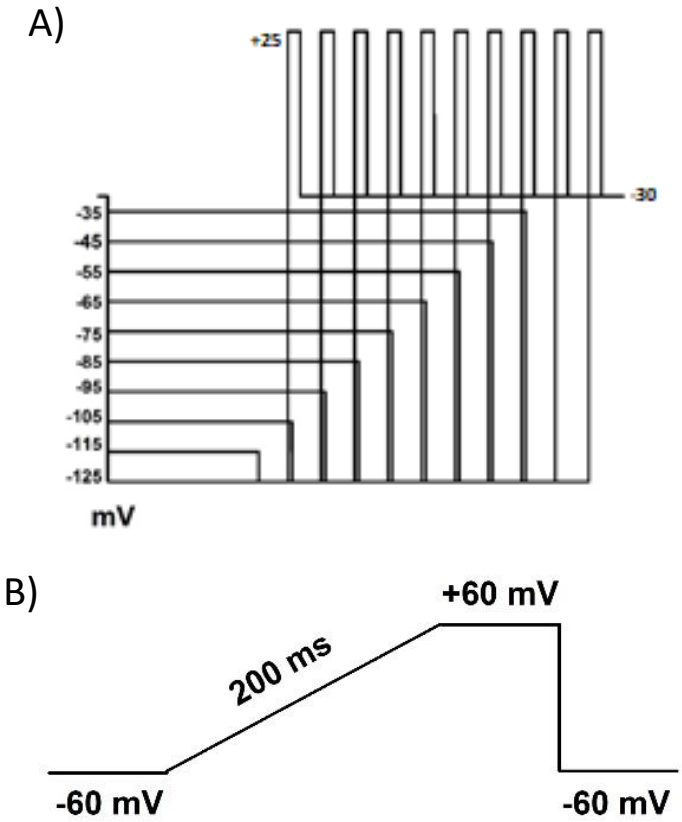

Figure 2. Voltage protocol used to record I_f (A) and I_{CaL} current (B).

Results

1. *Nfix expression in the heart*

I. Nfix gene expression during cardiac development.

To obtain detectable RNA during embryogenesis, different hearts samples for every time point considered were pulled together (embryonic day E, number of hearts: E10.5-12.5: n=6; E14.5-16.5: n=4; postnatal day P, P1: n=3; P3: n=2; P5: n=2; P7: n=2; adult ventricle, AV, n=1). Plotting the expression level at the various time points, a time course of *Nfix* expression in the heart from mid-gestation to adulthood was obtained (Figure 1, A). *Nfix* transcript is not expressed at around E10.5 ($2^{-\Delta Ct}$*100= 0.05, n=1). It displays an increase during development (E12.5: $2^{-\Delta Ct}$*100=0.66, n=1; E14.5: $2^{-\Delta Ct}$*100=1.10, n=1; E16.5: $2^{-\Delta Ct}$*100=1.67, n=1) and a peak of expression after birth (P1: $2^{-\Delta Ct}$*100= 2.00±0.79, n=3; P3: $2^{-\Delta Ct}$*100= 2.74±0.60, n=3; P5: $2^{-\Delta Ct}$*100= 2.95±0.22, n=3). At P7 *Nfix*-mRNA expression stabilizes to the value ($2^{-\Delta Ct}$*100= 3.36±0.37 n=3) that is maintained up to adulthood ($2^{-\Delta Ct}$*100=3.34±0.29, n=6).

II. Nfix gene expression in the adult heart.

Since *Nfix* transcript increases after birth, *Nfix* gene expression was investigated in the adult heart. In the adult mice, *Nfix* mRNA is not detected in *Nfix*-null tissues as expected, but it is in the heart, in the skeletal muscle and in the brain (Figure 1, B). *Nfix* transcript is expressed in the atria ($2^{-\Delta Ct}$*100= 40.66±7.2, n=6) and ventricles ($2^{-\Delta Ct}$*100= 48.37±5.30, n=6) to levels comparable to those of the tibialis muscle ($2^{-\Delta Ct}$*100= 36.68±19.34, n=3) and hippocampus ($2^{-\Delta Ct}$*100= 63.59±26.46, n=3). As evident from figure 1B, there are differences among the various cardiac regions: *Nfix* is

significantly less expressed in the SAN than ventricles and atria ($2^{-\Delta Ct}$*100=5.21±1.10*, n=6, *p<0.05 ANOVA Fisher's LSD) (Fig.1, B).

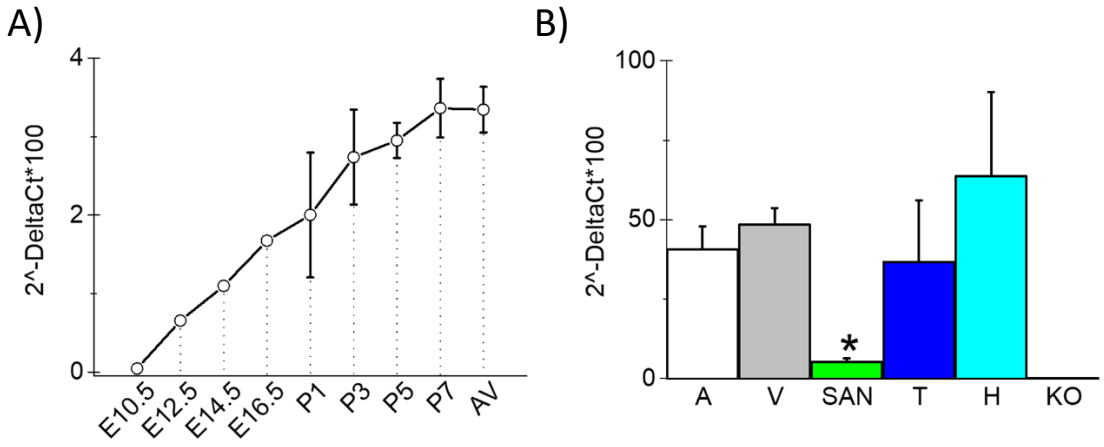

Figure 1. A) Time course of Nfix*-mRNA expression by qPCR during heart development (E= Embryonic Day; P= Post-Natal Day; AV= Adult Ventricles) B) Mean* Nfix *expression levels in the various regions of the heart (A= atria, V= ventricles, SAN= sinoatrial node) and in tibialis muscle (T), hippocampus (H) and* Nfix*-null ventricle (KO) for comparison.*

2. Cardiac morphology of WT and Nfix*-null mice*

Considering that *Nfix*-null mice are characterized by a reduced body size and distinctive skeletal defects (Campbell et al., 2008, Driller et al., 2007), we investigated the morphological characteristics of the heart of *Nfix*-null and WT mice. Histological analysis were performed on fixed heart sections obtained from 3-month-old *Nfix*-null (n=2) and WT mice (n=2). The sections were stained with either Hematoxylin&Eosin or Milligan's trichrome stain to highlight the presence of necrosis, hypertrophy or fibrosis. No evident morphological differences between *Nfix*-null and WT emerged suggesting that the structure of the heart is normal in the absence of NFIX (Fig. 2A).Since NFIX plays a pivotal role in skeletal sarcomere organization (Messina et al., 2010), alterations of myocardium-specific genes were investigated by qPCR in atria and ventricles of adult WT and *Nfix*-null mice. We considered the expression of the sarcomeric genes troponin (*cTnI*), myosins (*Mlc2v*, *Myh6* and *Myh7*) and of the transcription factor *Nkx2.5*, which is important for working myocardium commitment. As shown in figure 2B and in table 1, no statistical differences were found between the expression values of these genes in both atria and ventricles of *Nfix-null* and WT mice suggesting that sarcomere structure is not affected by the lack of NFIX protein.

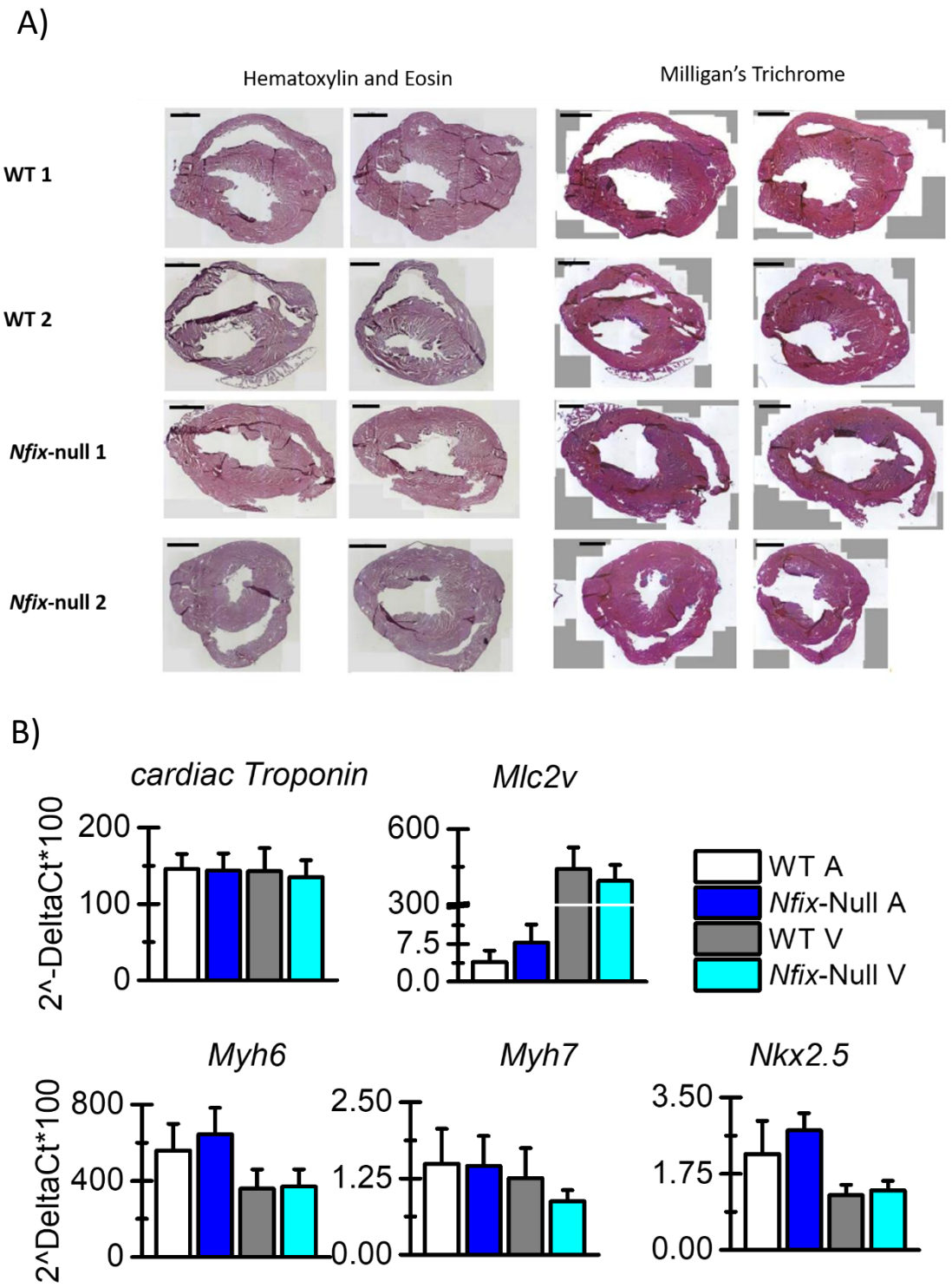

Figure 2. A) Histological sections of two WT and two Nfix*-null hearts stained by either Hematoxylin and Eosin stain or Milligan's Trichrome staining. Calibration bar=1 mm. B) Mean expression value of cardiac troponin I (*cTnI*), ventricular myosin light chain 2 (*Mlc2v*), Myosin heavy chain 6 (*Myh6*), 7 (*Myh7*) and NK2 Homeobox 5 (*Nkx2.5*) genes in WT and* Nfix*-null atria and ventricles.*

	WT ATRIA (n=3)	*Nfix*-null ATRIA (n=3)	WT VENTRICLES (n=3)	*Nfix*-null VENTRICLES (n=3)
cTnI	145.76± 19.79	143.57± 22.54	142.89± 30.14	135.28± 21.89
Mlc2v	3.94±2.30	3.94±2.30	440.00±86.88	392.68±63.37
Myh6	559.77±139.33	644.44±138.40	358.45±101.90	370.07±90.45
Myh7	1.49±0.58	1.46±0.49	1.26±0.49	0.87±0.19
Nkx2.5	2.20±0.77	2.75±0.39	1.25±0.25	1.37±0.22

Table 1. Mean expression value of cardiac troponin I (cTnI), ventricular myosin light chain 2 (Mlc2v), Myosin heavy chain 6 (Myh6), 7 (Myh7) and NK2 Homeobox 5 (Nkx2.5) genes in WT and Nfix-null atria and ventricles. All the mean values are expressed as $2^{-\Delta Ct}$**100±S.E.M; Student T-test was used to perform statistical analysis.*

3. NFIX loss increases intrinsic heart rate.

We then evaluated the effect of the lack of NFIX on the cardiac function in 6-month-old WT and *Nfix*-null mice were implanted with a radio transmitter and ECGs were recorded in freely moving conditions for 5 days. In Figure 3A, representative traces of ECGs recorded of WT (green) and *Nfix*-null (blue) mice are shown, in which a tachycardia is clearly visible. In panel B, timecourse of mean heart rate of *Nfix*-null (n=4) and WT (n=5) mice during 5 days of recordings are shown. Both WT and *Nfix*-null mice show a physiological increase of heart rate during night recordings following the circadian rhythm, but this change in rate is higher in *Nfix*-null (Δbpm=70±11.48*, n=16, *p=0.0006) than in WT (Δbpm=19.84±7.92, n=22) mice (Figure 3B). Moreover, *Nfix*-null shows a higher mean heart rate than WT both at night (WT: 496.70±13.07 bpm, n=22/5; *Nfix*-null: 587.48±8.68 bpm, n=18/4) and during the day (WT: 466.98±8.42 bpm n=24/5; *Nfix*-null: 523.10±13.25 bpm, n=17/4)(Figure 3C).

To understand if the *in vivo* tachycardia is an effect intrinsic of the pacemaker tissue or instead is due to a sympathetic hyperstimulation, pacemaker cells from the sinoatrial node (SANCs) were isolated for *in vitro* electrophysiological experiments. Representative trace of action potentials recorded in WT (green) and *Nfix*-null (blue) SANCs cells are depicted in Figure 4A. *Nfix*-null SANCs exhibit a higher firing rate (577.80±52.80 bpm*, n=7,*p=0.02) than WT-SANCs (403.80±45.00 bpm, n=7) suggesting that *in vivo*-tachycardia is associated with an increased intrinsic heart rate, independent of the autonomic tone (Figure 4B). Action potential amplitude (APA), Maximum Diastolic Potential (MDP) and Action Potential Duration at 50% of repolarization (APD50) were analyzed but no statistical differences emerged between *Nfix*-null and WT-SANCs (Table 2).

Because of the limited number of *Nfix*-null mice, another *in vitro* cellular model was used to study the effect of NFIX loss on cardiac rate. Neonatal rat ventricular cardiomyocytes (NRVCs), cells that show spontaneous beating, (Scavone et al., 2013) were infected with a lentivirus with either a short hairpin that downregulated *Nfix*-mRNA (*Nfix*-sh) or a scrambled sequence (Scramble). Using non-infected NRVCs as a control, we demonstrated that *Nfix*-sh infection caused an 85.24±2.26% (n=18) downregulation of the *Nfix* transcript (Figure 5A). Representative traces of spontaneous action potentials of both Scramble (green) and *Nfix*-sh (blue) are shown in figure 5B. *Nfix*-sh NRVCs display a higher action potential firing rate (87.60±7.80 bpm*, n=20, p=0.041) than Scramble cells (54.00±9.00 bpm, n=19). No differences were found in APA, MDP and APD50 between *Nfix*-sh and Scramble as shown in Table 3.

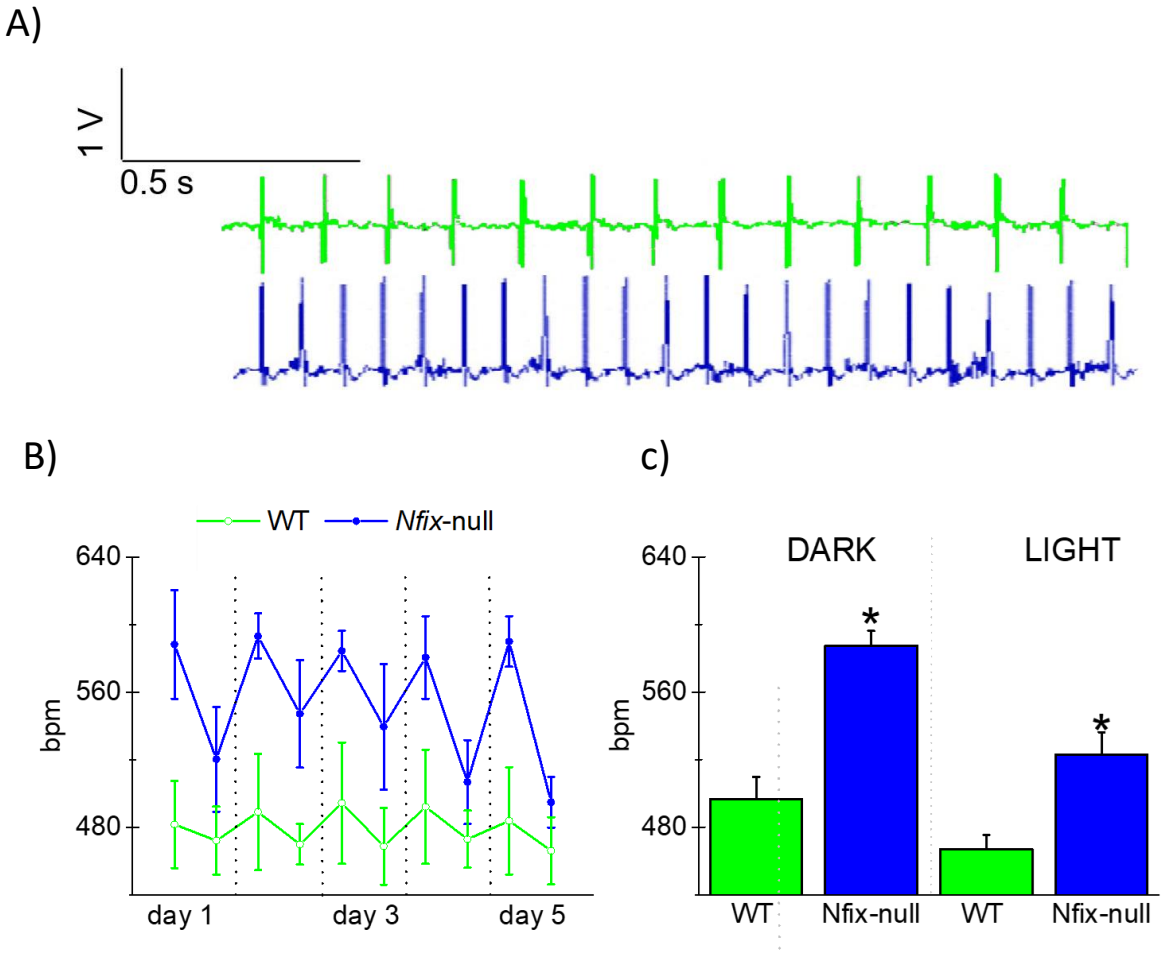

Figure 3. A) Representative ECGs traces recorded from freely moving WT (green) and Nfix-*null (blue) mouse. B) Timecourse of mean heart rate of WT and* Nfix-*null mice during 5 days of recordings C) Mean heart rate of dark and light recordings of WT and* Nfix-*null mice.*

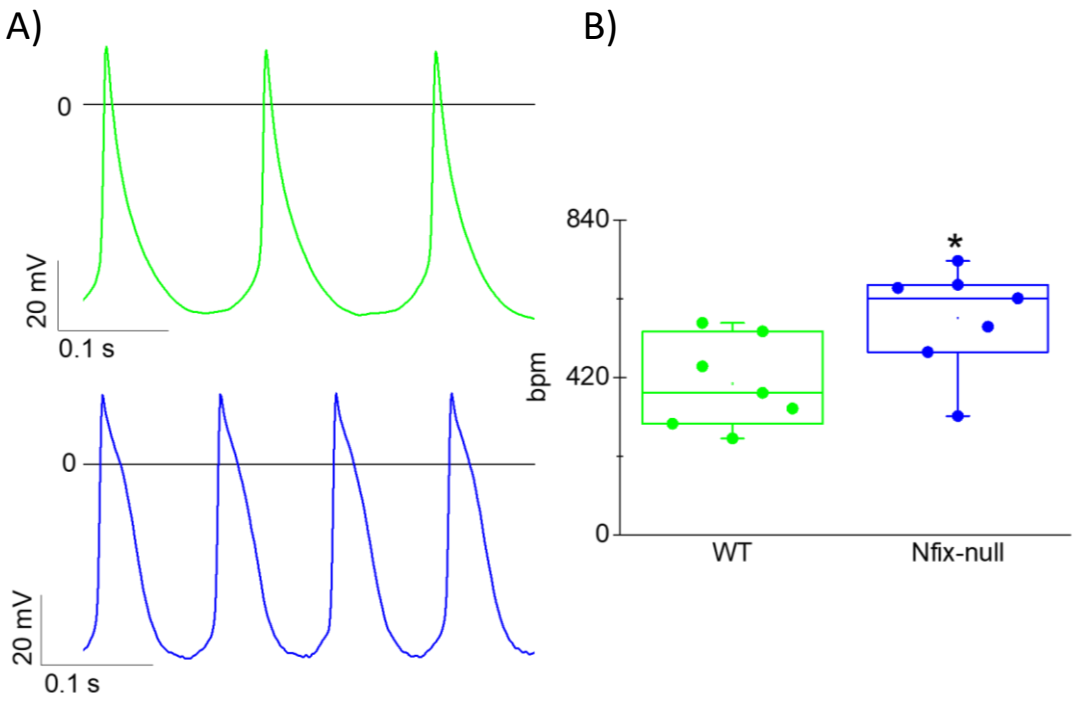

Figure 4. A) Representative spontaneous action potential traces of isolated WT and Nfix*-null SANCs. B) Boxplot of mean action potential firing rate of WT and* Nfix*-null cells.*

	APA (mV)	**MDP (mV)**	**APD50 (ms)**
WT (n=7)	79.15±12.44	-57.90±3.55	28.61±3.54
***Nfix*-null (n=7)**	75.66±5.35	-58.92±3.13	24.12±1.42

Table 2. Spontaneous Action Potential parameters in Nfix-null and WT SANCs.

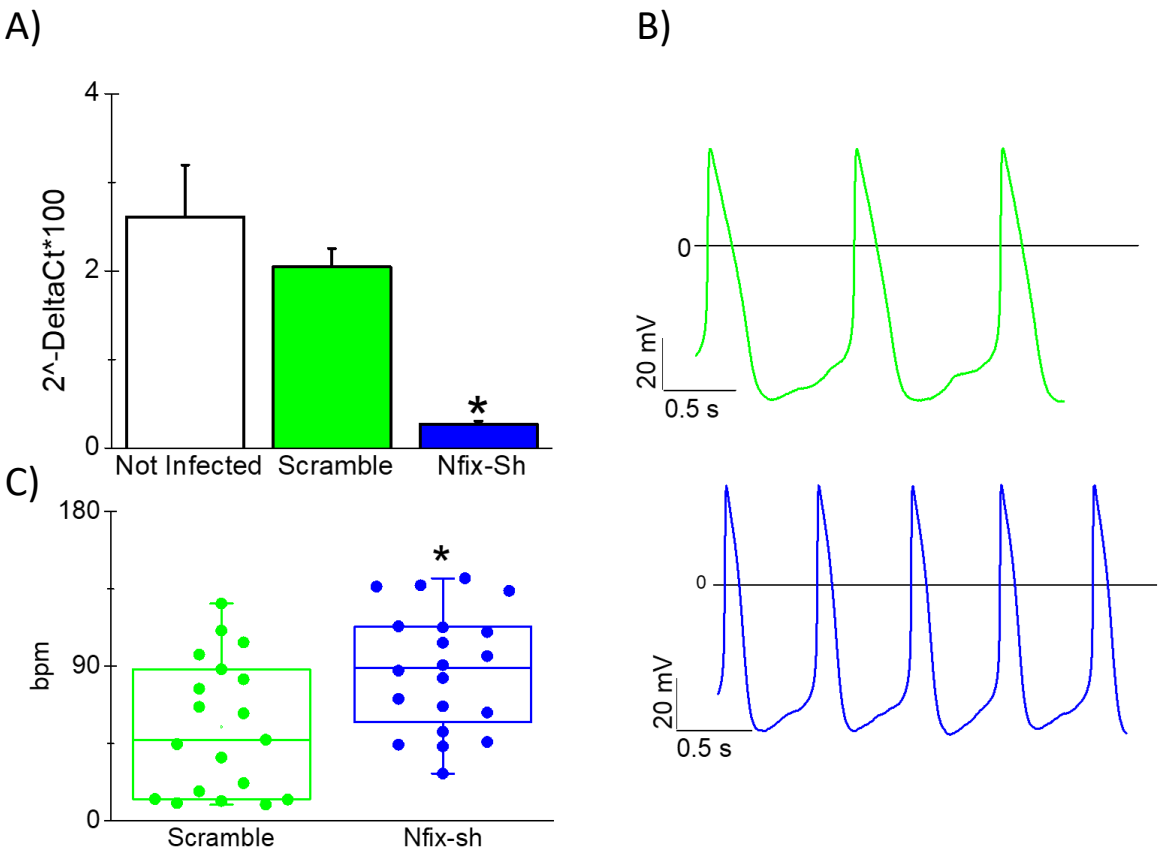

Figure 5. A) Mean Nfix-*transcript expression in Not Infected, Scramble and* Nfix-*sh NRVCs; ANOVA Fisher's LSD, *p<0.05. B) Spontaneous action potentials recorded from Scramble (green) and* Nfix-*sh (blue) NRVCs. C) Boxplot of APs firing rate in scramble and* Nfix-*sh NRVCs; Student's T-test, *p<0.05.*

	APA (mV)	**MDP (mV)**	**APD50 (ms)**
Scramble (n=19)	92.82±3.25	-59.22±1.75	107.68±5.92
***Nfix*-sh (n=20)**	93.45±3.25	-57.30±2.19	100.97±8.62

Table 3. Spontaneous Action Potential parameters in Nfix-sh and Scramble NRVCs.

4. NFIX loss enhances CAV1.3- L-Type Calcium current but does not affect Funny current.

Action potential firing originates from a combination of pacemaker currents involved during the diastolic depolarization of the action potential including the funny current (I_f) and L-type calcium current (I_{CaL}). To clarify the role of these ion channels in *Nfix*-null mouse model's tachycardia, we performed an analysis of the abundance of both the sinoatrial f-channels *Hcn4* and the sinoatrial calcium channels isoforms in *Nfix*-null and WT SAN including L-type (*Cacna1c* and *Cacna1d*) and T-type (*Cacna1g* and *Cacna1h*) calcium channels (Figure 6). We found an upregulation of *Hcn4* (Fig. 6A) and *Cacna1d* (Fig. 6B) transcript in *Nfix*-null (*Hcn4:* $2^{-\Delta Ct}$*100= 0.94±0.21*, n=5; *Cacna1d:* $2^{-\Delta Ct}$*100=1.45±0.40*, n=5) compared to WT (*Hcn4:* $2^{-\Delta Ct}$*100=0.40±0.03, n=5; *Cacna1d:* $2^{-\Delta Ct}$*100=0.59±0.12, n=8) SAN tissues. For this reason, we perform an electrophysiological characterization of both funny and L-type calcium current in our cellular models of murine SANCs and NRVCs. In figure 7A and D, representative traces of recorded I_f in both SAN and NRVC cellular models are shown. In contrast of the apparent *Hcn4*-mRNA upregulation in *Nfix*-null SAN, there were no statistical differences in neither current density nor kinetics in WT vs *Nfix*-null cells (Figure 7B and C) and Scramble vs *Nfix*-sh NRVCs (Figure 7E and F)(Table 4) suggesting that *Nfix*-null's tachycardia is not caused by a gain-of-function of I_f current. Representative traces of Nifedipine-sensitive I_{CaL} current from Scramble and *Nfix*-sh NRVCs revealed an increase of I_{CaL} density current in *Nfix*-sh (Figure 8A). *Nfix*-sh exhibits a higher I_{CaL} current density amplitude (at 0mV: -2.19±0.24, n=11) than Scramble (at 0mV: -1.42±0.19, n=5) NRVCs (Figure 8B).

Considering that only *Cacna1d* transcript was found to be upregulated in *Nfix*-null compared to WT SAN we hypothesize an increase of CaV1.3 L-type calcium current in the knockout model that we would like to confirm in the next electrophysiological experiments in SANCs.

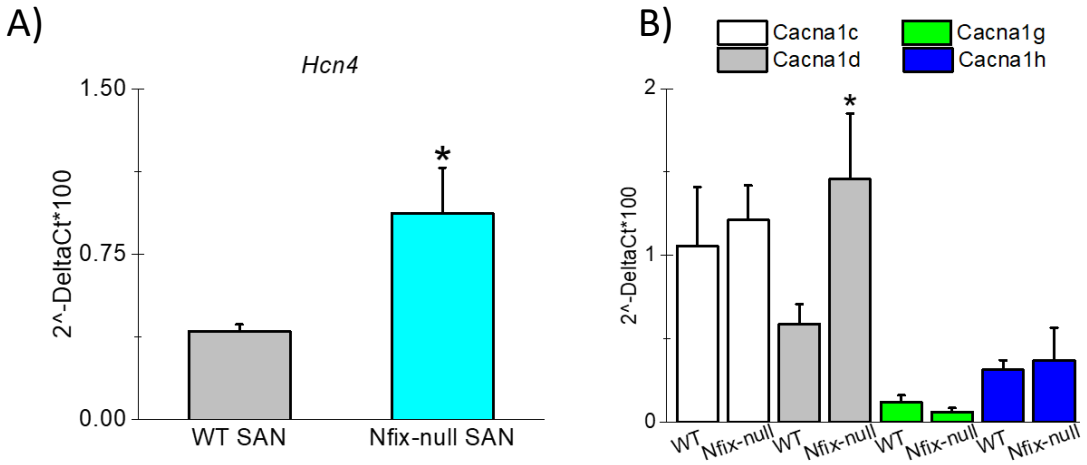

*Figure 6. Mean expression value of Hcn4 (A), L-type (*Cacna1c *and* Cacna1d*) and T-type (*Cacna1g *and* Cacna1h*) in WT and* Nfix*-null SAN tissue (B).*

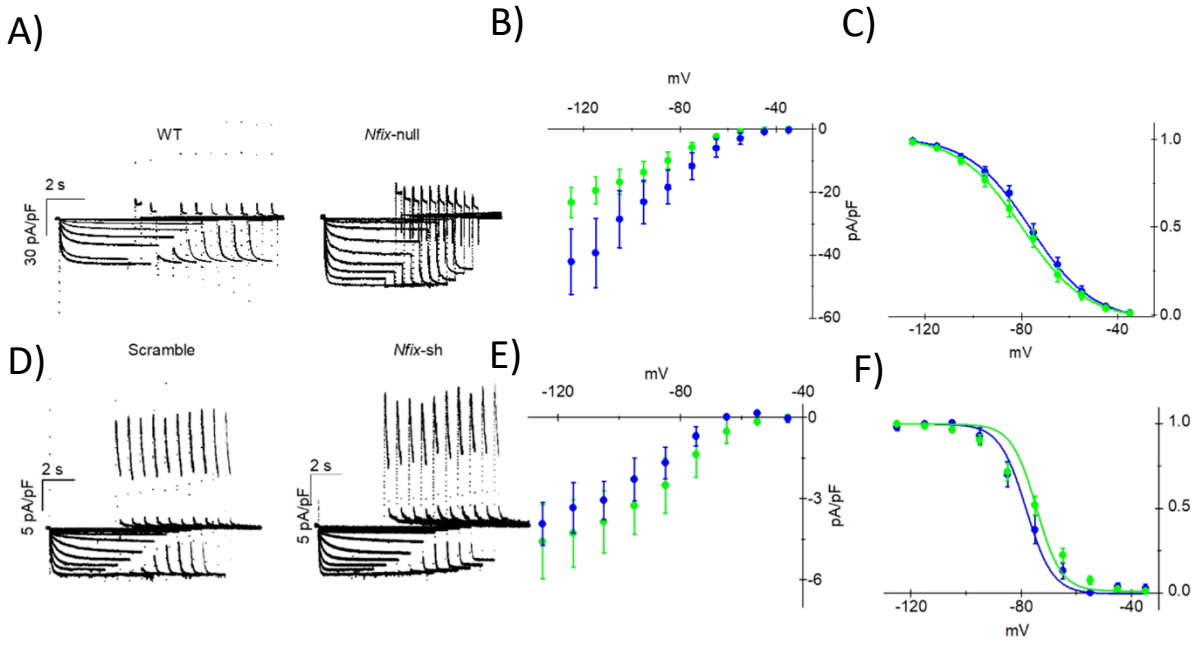

Figure 7. A&D) Representative traces of recorded funny current of WT vs Nfix*-null SANCs (A) and Scramble and* Nfix*-sh infected NRVCs (D). B&E) Mean I_f current density vs voltages of WT vs* Nfix*-null SANCs (B) and Scramble and* Nfix*-sh infected NRVCs (E). C&F) Mean I_f activation curve of WT vs* Nfix*-null SANCs (C) and Scramble and* Nfix*-sh infected NRVCs (F).*

	Current density at -125mV (pA/pF)	V_{half} (mV)	Slope
WT	-23.25±4.78 (n=9)	-79.19±2.29 (n=15)	10.85±0.64 (n=15)
***Nfix*-null**	-42.11±10.34 (n=13)	-75.42±2.10 (n=14)	10.15±0.67 (n=14)
Scramble	-4.57±1.37 (n=4)	-75.78±1.63 (n=9)	7.55±0.89 (n=9)
***Nfix*-sh**	3.92±0.80 (n=5)	-79.01±1.94 (n=5)	6.03±0.81 (n=5)

Table 4. I_f parameters analysis in SAN and NRVC cellular models. While for current density, only single cells were considered, for activation curve analysis even small groups of cells were included.

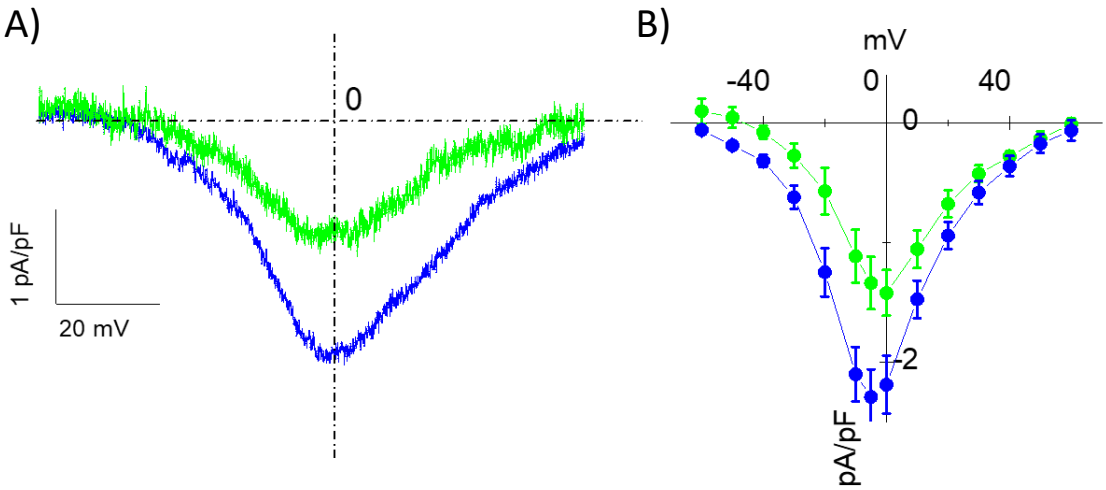

Figure 8. A) Representative traces of recorded Nifedipine-sensitive I_{CaL} in Scramble (green) and Nfix-*sh (blue). B) Mean I_{CaL} current density in Scramble and* Nfix-*sh. C) Mean expression value of*

Discussion

The Nuclear Factor I (NFI) transcription factor family (NFIA, NFIB, NFIC and NFIX) has many roles in animal physiology, biochemistry and pathology (Gronostajski et al., 2000). Gene deletion technologies elucidated the importance of these genes in several tissues such as brain, lungs, teeth, intestine, muscle and skeleton (das Neves et al., 1999, Campbell et al., 2008, Driller et al., 2007). *Nfix*-null mice exhibit several evident anomalies including reduced body size (Campbell et al., 2008, Driller et al., 2007), severe fiber disorganization of the skeletal muscle (Messina et al., 2010) and a reduced size of the cerebellum (Piper et al., 2011). Although, *Nfix* transcript has been demonstrated to be present in other tissues in the mouse (Chaudry et al., 1997), the full spectrum of functions of this transcription factor is still unclear. Recently, *loss-of-function* mutations of *NFIX* gene have been associated with the onset of rare overgrowth syndromes (Malan and Marshall-Smith syndromes) in humans that resemble for many aspects the Nfix *knock-out* mouse phenotype (Malan et al., 2010, Driller et al., 2007). For this reason, the interest about the role of this transcription factor is growing and needs to be unravelled.

The first evidence about the role of NFIX has been gathered during the development of the brain and the skeletal muscle (Messina et al., 2010, Matuzelski et al., 2017).
In the skeletal muscle, Messina and colleagues demonstrated that NFIX plays a pivotal role in the transcriptional switch from the primary embryonic muscle into a more mature and organized fetal muscle inhibiting the expression of the slow myosin heavy chain protein (Messina et al., 2010).

We demonstrated that in the heart, *Nfix* expression gradually increases during development reaching the peak of expression around birth and thereafter it is maintained in adulthood. The exponential increase of *Nfix*-mRNA seems to parallel the increase of *Myh6*-mRNA and the decrease of *Myh7*-mRNA during the cardiac development as shown by Willie and colleagues (Willie et al., 1991). This evidence suggests that similarly to what happens during skeletal myogenesis, NFIX may participate in the transcriptional switch between *Myh7* and *Myh6* in the heart. However, we did not find evident cardiac alterations between WT and *Nfix*-null mice despite the defects in the skeletal muscle in *Nfix*-null mice (Messina et al., 2010).

In the adult mouse, it has been shown that NFIX promotes the regeneration process of the skeletal muscle after injury through the inhibition of the Myostatin pathaway (Rossi et al., 2016) and the neural stem cell differentiation in the hippocampus (Harris et al., 2018). In this study, we demonstrated that *Nfix* gene is expressed in the adult heart comparably to the tibialis muscle and the hippocampus. Notably, in the heart *Nfix* is highly expressed in the atria and the ventricles that constitute the working myocardium. The evidence that *Nfix*-mRNA is abundant in the working myocardium strengthens the idea that NFIX could regulate the expression of structural proteins important for the contraction activity of the heart. In the skeletal muscle, NFIX is able to modulate myosins promoter activity alone (Messina et al., 2010) or together with other transcription factors (Taglietti et al., 2016). Contrarily , in the heart several genes that are specifically expressed in the working myocardium, such as cardiac troponin I (cTNI), atrial and ventricular specific myosins (MYH6, MYH7 and MLCV2) and the

transcription factor NKX2.5, do not show statistical differences of expression levels in WT and *Nfix*-null cardiac tissues.

We observed that in the sinoatrial node (SAN), where the heartbeat originates, *Nfix* transcript, although present, is significantly less expressed than in the working myocardium. ECGs recorded from freely moving WT and *Nfix*-null mice indicated that the absence of the NFIX protein leads to tachycardia during both day and night, strongly suggesting a link to electrical alterations in the heart. It has been shown that transcription factors can be linked to electrical alterations in the heart. For example, several variants associated with atrial fibrillation appear in proximity of the *PITX2* gene (Gudbjartsson et al., 2007) that encodes for a transcription factor essential for the transcriptional block of SAN development in the left atrium (Mommersteeg et al., 2008).

To properly clarify the connection between *in vivo* tachycardia and NFIX loss, we considered that physiologically tachycardia could be caused by either an enhancement of the activity of the sympathetic nervous system or by an increase of the intrinsic heart rate in SAN. SAN cells isolated from *Nfix*-null mice display a higher action potential firing rate in comparison to WT-SANCs. These *in-vitro* experiments clearly demonstrate that *in vivo* tachycardia is not dependent on sympatho-vagal regulation, but rather a direct effect of the increase of intrinsic SANCs rate. To confirm this hypothesis and exclude sympatho-vagal involvement, in the next experiments we will also consider the heart rate variability from ECGs recordings. Furthermore, to investigate the NFIX-dependent tachycardia, RNA interference was performed on neonatal rat ventricular cardiomyocytes (NRVCs) to specifically silence *Nfix* gene. NRVCs are immature ventricular cardiomyocytes that maintain a spontaneous beating activity similarly to

pacemaker cells making them an attractive *in-vitro* cellular model (Campostrini et al., 2017, Scavone et al., 2013). Similarly to SANCs, *Nfix*-silenced NRVCs (*Nfix*-SH) display an higher action potentials rate in comparison to scrambled-infected NRVCs (Scramble) confirming that NFIX is able to negatively modulate the intrinsic cellular rate.

The reduction of the expression level of *Nfix* gene thus leads to an increase of action potential firing rate. Our hypothesis is that NFIX acts as a negative modulator of pacemaker activity and *Nfix* mRNA expression must be lower in the SAN than the working myocardium to allow pacemaking. This hypothesis is further confirmed by the analysis of *Nfix*-mRNA expression levels comparing adult mouse heart and NRVCs. NRVCs show a higher *Nfix* expression than SAN tissue but still lower than working myocardium (data not shown) suggesting that spontaneous beating activity of the immature myocytes disappears in the adult working myocardium because of the increase of *Nfix* transcription.

Alterations of the physiological intrinsic heart rate can be explained by changing the slope of the slow diastolic depolarization phase which is primarily sustained by the Funny current (I_f) (DiFrancesco et al., 1986, Baruscotti et al., 2005, Barbuti et al., 2007) and/or I_{CaT} and I_{CaL} calcium currents (Mangoni et al., 2003, Mangoni et al., 2006, Mesirca et al., 2014). We investigated the expression levels of several sinoatrial ion channels involved in the diastiolic depolarization in WT and *Nfix*-null SAN tissues. We found that only *Hcn4* and *Cacna1d* mRNAs were upregulated in the *Nfix*-null SAN. HCN4 is the most abundant HCN channel in SAN and it sustains the I_f current (Brioschi et al., 2009). In the literature, HCN4 mutations have also been linked to alterations of heart rate including sinus bradycardia (Milanesi et al., 2006) and tachycardia (Baruscotti et al., 2017).

Baruscotti and collegues, for example, demonstrated also that *Hcn4*-KO mouse model display deep bradycardia due to I_f decrease in SAN (Baruscotti et al., 2011). Moreover, cardiomyocytes derived from the differentation of HCN4-overexpressing mouse embryonic stem cells (mESCs) show an enhancement of the spontaneous beating activity when compared with the WT mESCs (Saito et al., 2015). Neither *Nfix*-null- SAN cells nor *Nfix*-SH-infected NRVCs exhibit any significant differences in I_f kinetics or current density amplitudes when compared to their respective controls suggesting that HCN channels are not potential targets of NFIX activity.

The T-type calcium channels genes for CAV3.1 (*Cacna1g*) and CAV3.2 (*Cacna1h*) do not display any differences in their expression levels in *Nfix*-null and WT SAN tissues suggesting T-type calcium channels are not affected by NFIX regulation. The L-type calcium channels genes for CAV1.2 (*Cacna1c*) and CAV1.3 (*Cacna1d*) were also considered. We did not find any differences in *Cacna1c* expression in *Nfix*-null and WT SAN but *Cacna1d* was upregulated in *Nfix*-null SAN. Since CAV1.3 is the predominant L-type calcium channel isoform in SAN tissue and it gives the greater contribution to pacemaking mechanisms (Christel et al., 2012, Gao et al., 2011), NFIX-dependent action potential rate increase can be caused by an upregulation of L-type calcium current. Mangoni et al. showed that CAV1.3 KO SAN cells display a 60% reduction of I_{CaL} amplitude and slower action potential firing rate than WT SANCs (Mangoni et al., 2001, Mangoni et al., 2003, Rose et al., 2011). Furthermore, global CAV1.3 KO induces bradycardia and atrioventricular block in mouse model (Platzer et al., 2000, Marger et al., 2011). Electrophysiological experiments to study I_{CaL} amplitude and kinetics have not been performed in *Nfix*-null and WT SAN cells yet, but we demonstrated that I_{CaL} current density amplitude in *Nfix*-SH

NRVCs is higher than in *Scramble* NRVCs. The evidence that alterations in CAV1.3 channels modulate SAN rate is in accordance with the idea that a gain of function of CAV1.3 may consequently cause tachycardia. In conclusion, here we demonstrated for the first time that NFIX is not only expressed in the adult heart, but it also acts as a negative regulator of cardiac automaticity, presumably affecting CAV1.3 channels expression. In the skeletal muscle, Messina and colleagues consider NFIX as the key regulator of transcriptional switch from embryonic to fetal myogenesis. However, we discover a new potential role of NFIX in development. Our data suggest that the activation of the transcription of *Nfix* gene after birth is not a coincidence but rather a pivotal event for transition from pacemaking into not-pacemaking tissue during cardiac development.

References

Altman PL & DS Dittmer "Biological data book. Federation of American Societies for Experimental Biology" *Washington, District of Columbia*, 1964: 633 pp.

Altomare C, Terragni B, Brioschi C, Milanesi R, Pagliuca C, Viscorni C, Moroni A, Baruscotti M, DiFrancesco D. "Heteromeric HCN1-HCN4 channels: A comparison with native pacemaker channels from the rabbit sinoatrial node." *The Journal of Physiology,* 2003: 347-359.

Anderson C, Catoe H, Werner R "miR-206 regulates connexin43 expression during skeletal muscle development." *Nucleic Acids Res.*, 2006: 34(20):5863-71.

Barbuti A, Baruscotti M, DiFrancesco D. "The pacemaker current: from basics to the clinics." *J Cardiovasc Electrophysiol.*, 2007: 342-7.

Barbuti A, Robinson RB "Stem Cell–Derived Nodal-Like Cardiomyocytes as a Novel Pharmacologic Tool: Insights from Sinoatrial Node Development and Function." *Pharmacological Reviews*, 2015: 67:368–388.

Barrett PQ, Guagliardo NA, Klein PM, Hu C, Breault DT, Beenhakker MP. "Role of voltage-gated calcium channels in the regulation of aldosterone production from zona glomerulosa cells of the adrenal cortex." *J Physiol.*, 2016: 5851-5860. doi: 10.1113/JP271896.

Barry G, Piper M, Lindwall C, Moldrich R, Mason S, Little E, Sarkar A, Tole S, Gronostajski RM, Richards LJ. "Specific glial populations regulate hippocampal morphogenesis." *J Neurosci,* 2008: 28:12328–12340.

Baruscotti M, Bucchi A, DiFrancesco D. “Physiology and pharmacology of the cardiac pacemaker (“funny”) current.” *Pharmacology & Therapeutics*, 2005: 59-79.

Baruscotti M, DiFrancesco D. “Pacemaker channels.” *Ann N Y Acad Sci.* , 2004: 111-21.

Baruscotti M, Bucchi A, Viscomi C, Mandelli G, Consalez G, Gnecchi-Rusconi T, Montano N, Casali KR, Micheloni S, Barbuti A, DiFrancesco D. “Deep bradycardia and heart block caused by inducible cardiac-specific knockout of the pacemaker channel gene Hcn4.” *PNAS*, 2011: 108 (4) 1705-1710.

Baruscotti M, Bucchi A, Milanesi R, Paina M, Barbuti A, Gnecchi-Ruscone T, Bianco E, Vitali-Serdoz L, Cappato R, DiFrancesco D. “A gain-of-function mutation in the cardiac pacemaker HCN4 channel increasing cAMP sensitivity is associated with familial Inappropriate Sinus Tachycardia.” *Eur Heart J.*, 2017: Jan 21;38(4):280-288. doi: 10.1093/eurheartj/ehv582.

Betancourt J, Katzman S, Chen B. “Nuclear factor one B regulates neural stem cell differentiation and axonal projection of corticofugal neurons.” *J Comp Neurol*, 2014: 522:6–35.

Biel M, Schneider A, Wahl C. “Cardiac HCN Channels: Structure, Function, and Modulation.” *Medicine*, 2002: 206-213.

Bogdanov KY, Vinogradova TM, and Lakatta EG. “Sinoatrial nodal cell ryanodine receptor and Na(+)-Ca(2+) exchanger: molecular partners in pacemaker regulation.” *Circ. Res.* , 2001: 88, 1254–1258. doi: 10.1161/hh1201.092095.

Brioschi C, Micheloni S, Tellez JO, Pisoni G, Longhi R, Moroni P, Billeter R, Barbuti A, Dobrzynski H, Boyett MR, DiFrancesco D, Baruscotti M. “Distribution of the pacemaker HCN4 channel mRNA and protein in the rabbit sinoatrial node.” *J Mol Cell Cardiol.* , 2009: 221-7.

Brown HF, DiFrancesco D, Noble SJ. “How does adrenaline accelerate the heart?” *Nature*, 1979: 235-6.

Bucchi A, Tognati A, Milanesi R, Baruscotti M, DiFrancesco D. “Properties of ivabradine-induced block of HCN1 and HCN4 pacemaker channels.” *J Physiol.*, 2006: 335-346.

Campbell CE, Piper M, Plachez C, Yeh YT, Baizer JS, Osinski JM, Litwack D, Richards LJ, Gronostajski RM. “The transcription factor Nfix is essential for normal brain development.” *BMC Developmental Biology*, 2008: 8:52 doi:10.1186/1471-213X-8-52.

Campostrini G, Bonzanni M, Lissoni A, Bazzini C, Milanesi R, Vezzoli E, Francolini M, Baruscotti M, Bucchi A, Rivolta I5, Fantini M, Severi S, Cappato R, Crotti L, J Schwartz P, DiFrancesco D, Barbuti A. “The expression of the rare caveolin-3 variant T78M alters cardiac ion channels function and membrane excitability.” *Cardiovasc Res.* , 2017: Aug 1;113(10):1256-1265. doi: 10.1093/cvr/cvx122.

Catterall WA. “Structure and regulation of voltage-gated Ca2+ channels.” *Annu Rev Cell Dev Biol.,* 2000: 16:521-55.

Cerbai E, Mugelli A. “I(f) in non-pacemaker cells: role and pharmacological implications.” *Pharmacol Res.,* 2006: May;53(5):416-23. Epub 2006 Mar 28.

Chaudry AZ, Lyons GE, Gronostajski RM. “Expression Patterns of the Four Nuclear Factor I Genes During Mouse Embryogenesis Indicate a Potential Role in Development.” *Developmental Dynamics*, 1997: 208:313-325.

Chen J, Mitcheson JS, Tristani-Firouzi M, et al. “The S4–S5 linker couples voltage sensing and activation of pacemaker channels.” *Proc Natl Acad Sci USA*, 98 (2001), pp. 11,277-11,282

Choisy SC, Cheng H, Orchard CH, James AF, Hancox JC. “Electrophysiological properties of myocytes isolated from the mouse atrioventricular node: L-type ICa, IKr, If, and Na-Ca exchange.” *Physiol Rep.* , 2015: pii: e12633. doi: 10.14814/phy2.12633.

Christel CJ, Cardona N, Mesirca P, Herrmann S, Hofmann F, Striessnig J, Ludwig A, Mangoni ME, Lee A. “Distinct localization and modulation of Cav1.2 and Cav1.3 L-type Ca2+ channels in mouse sinoatrial node.” *J Physiol.*, 2012: Dec 15;590(24):6327-42. doi: 10.1113/jphysiol.2012.239954. Epub 2012 Oct 8.

Cingolani E, Joshua I, Goldhabe, Marbán E. “Next-generation pacemakers: from small devices to biological pacemakers.” *Nature Reviews Cardiology*, 2018: 15:139-150.

das Neves L, Duchala CS, Tolentino-Silva F, Haxhiu MA, Colmenares C, Macklin WB, Campbell CE, Butz KG., Gronostajski RM. “Disruption of the murine nuclear factor I-A gene (Nfia) results in perinatal lethality, hydrocephalus, and agenesis of the corpus callosum.” *Proc Natl Acad Sci U S A*, 1999: 96:11946–11951.

Denyer JC, Brown HF. “Pacemaking in rabbit isolated sino-atrial node cells during Cs+ block of the hyperpolarization-activated current if.” *J Physiol.* , 1990: 401-9.

DiFrancesco D, Mangoni M. “Modulation of single hyperpolarization-activated channels (if) by cAMP in the rabbit sino-atrial node.” *J Physiol.* , 1994: Feb 1;474(3):473-82.

DiFrancesco D, Ferroni A, Mazzanti M, Tromba C. “Properties of the hyperpolarizing-activated current (if) in cells isolated from the rabbit sino-atrial node.” *The Journal of Physiology*, 1986: 377, 61–88.

DiFrancesco, D. “A study of the ionic nature of the pace-maker current in calf Purkinje fibres.” *J Physiol*, 1981: 377-393.

Dobrzynski H, Anderson RH, Atkinson A, Borbas Z, D'Souza A, Fraser JF, Inada S, Logantha SJ, Monfredi O, Morris GM, Moorman AF, Nikolaidou T, Schneider H, Szuts V, Temple IP, Yanni J, Boyett MR. “Structure, function and clinical relevance of the cardiac conduction system, including the atrioventricular ring and outflow tract tissues. .” *Pharmacology and Therapeutics*, 2013: 139(2), 260–288.

Driller K, Pagenstecher A., Uhl M., Omran H., Berlis A., Gründer A., Sippel A.E. “Nuclear factor I X deficiency causes brain malformation and severe skeletal defects.” *Mol Cell Biol*, 2007: (10), 3855-3867.

Gao Z, Singh MV, Hall DD, Koval OM, Luczak ED, Joiner ML, Chen B, Wu Y, Chaudhary AK, Martins JB, Hund TJ, Mohler PJ, Song LS, Anderson ME.. “Catecholamine-Independent Heart Rate Increases Require CaMKII.” *Circulation. Arrhythmia and Electrophysiology*, 2011: 4(3), 379–387. http://doi.org/10.1161/C.

Gauss R, Seifert R, Kaupp UB "Molecular identification of a hyperpolarization-activated channel in sea urchin sperm." *Nature*, 393 (1998), pp. 583-587

Gounari F, De Francesco R., Schmitt J., van der Vliet P, Cortese R, Stunnenberg H. "Amino-terminal domain of NFI binds to DNA as a dimer and activates adenovirus DNA replication." *EMBO J.*, 1990: 9, 559-566.

Gronostajski RM. "Roles of the NFI/CTF gene family in transcription and development." *Gene*, 2000: 249:31–45.

Grunder A, Ebel TT, Mallo M, Schwarzkopf G, Shimizu T, Sippel AE, Schrewe H. "Nuclear factor I-B (Nfib) deficient mice have severe lung hypoplasia." *Mech Dev*, 2002: 112:69–77.

Gudbjartsson DF, Arnar DO, Helgadottir A, Gretarsdottir S, Holm H, Sigurdsson A, Jonasdottir A, Baker A, Thorleifsson G, Kristjansson K, Palsson A, Blondal T, Sulem P, Backman VM, Hardarson GA, Palsdottir E, Helgason A, Sigurjonsdottir R, Sverrisson JT,. "Variants conferring risk of atrial fibrillation on chromosome 4q25." *Nature*, 2007: Jul 19;448(7151):353-7. Epub 2007 Jul 1.

Guehmann S, Vorbrueggen G, Kalkbrenner F, Moelling K. "Reduction of a conserved Cys is essential for Myb DNA-binding." *Nucleic Acids Res.*, 1992: 20, 2279-2286.

Hagiwara N, Irisawa H and Kameyama M. "Contribution of two types of calcium currents to the pacemaker potentials of rabbit sino-atrial node cells." *J Physiol.*, 1988: 233-253.

Harris L, Zalucki O, Clément O, Fraser J, Matuzelski E, Oishi S Harvey TJ, Burne THJ, Heng JI, Gronostajski RM, Piper M. “Neurogenic differentiation by hippocampal neural stem and progenitor cells is biased by NFIX expression.” *Development.*, 2018: Feb 7;145(3). pii: dev155689. doi: 10.1242/dev.155689.

Harris L, Zalucki O, Gobius I, McDonald H, Osinki J, Harvey TJ, Essebier A, Vidovic D, Gladwyn-Ng I, Burne TH, Heng JI, Richards LJ, Gronostajski RM, Piper M. “Transcriptional regulation of intermediate progenitor cell generation during hippocampal development.” *Development,* 2016: 15;143(24):4620-4630.

Hell JW, Westenbroek RE, Warner C, Ahlijanian MK, Prystay W, Gilbert MM, Snutch TP, Catterall WA. “Identification and differential subcellular localization of the neuronal class C and class D L-type calcium channel α1 subunits.” *J Cell Biol.* , 1993: Nov;123(4):949-62.

Herrmann S, Layh B, Ludwig A. “Novel insights into the distribution of cardiac HCN channels: an expression study in the mouse heart.” *J Mol Cell Cardiol.*, 2011: 997-1006.

Hoogaars WM, Engel A, Brons JF, Verkerk AO, de Lange F.J., Wong LY, Bakker ML., Clout DE, Wakker V, Barnett P, et al. “Tbx3 controls the sinoatrial node gene program and imposes pacemaker function on the atria.” *Genes Dev*, 2007: 21:1098–1112.

Hoogaars WM, Tessari A, Moorman AF, de Boer PA, Hagoort J. Soufan AT, Campione M., Christoffels V.M. “The transcriptional repressor Tbx3 delineates the developing central conduction system of the heart.” *Cardiovascular Research,* 2004: 62:489-499.

Hume JR, Grant AO. *Agents used in cardiac arrhythmias (Chapter 14). Basic and Clinical Pharmacology. 12e.* McGraw-Hill / Lange., 2012.

Kim HK, Lee YS, Sivaprasad U, Malhotra A, Dutta A. "Muscle-specific microRNA miR-206 promotes muscle differentiation." *J Cell Biol.*, 2006.

Kleemann M, Schneider H, Unger K, Sander P, Schneider EM, Fischer-Posovszky P, Handrick R, Otte K. "MiR-744-5p inducing cell death by directly targeting HNRNPC and NFIX in ovarian cancer cells." *Sci Rep.*, 2018: 8(1):9020.

Kodama I, Nikmaram MR, Boyett MR, Suzuki R, Honjo H, Owen JM. "Regional differences in the role of the Ca2+ and Na+ currents in pacemaker activity in the sinoatrial node." *Am J Physiol.* , 1997: Jun;272(6 Pt 2):H2793-806.

Koschak A, Reimer D, Huber I, Grabner M, Glossmann H, Engel J, Striessnig J. "alpha 1D (Cav1.3) subunits can form l-type Ca2+ channels activating at negative voltages." *J Biol Chem.* , 2001: Jun 22;276(25):22100-6. Epub 2001 Apr 2.

Kotturi MF, Carlow DA, Lee JC, Ziltener HJ, Jefferies WA. "Identification and functional characterization of voltage-dependent calcium channels in T lymphocytes." *J Biol Chem.* , 2003: Nov 21;278(47):46949-60. Epub 2003 Sep 3.

Kramer K, van Acker SA, Voss HP, Grimbergen JA, van der Vijgh WJ, Bast A. "Use of telemetry to record electrocardiogram and heart rate in freely moving mice." *J Pharmacol Toxicol Methods.*, 1993; 30: 209–215.

Krishnan A, Samtani R, Dhanantwari P, Lee E, Yamada S, Shiota K, Donofrio MT, Leatherbury L, Lo CW. “A detailed comparison of mouse and human cardiac development.” *Pediatr Res.*, 2014; Dec;76(6):500-7. doi: 10.1038/pr.2014.128. Epub 2014 Aug 28.

Lakatta EG, Maltsev VA and Vinogradova, TM. “A coupled SYSTEM of intracellular Ca2+ clocks and surface membrane voltage clocks controls the timekeeping mechanism of the heart's pacemaker.” *Circ. Res.*, 2010: 659–673. doi: 10.1161/CIRCRESAHA.109.206078.

Liu S, Qu D, Li W, He C, Li S, Wu G, Zhao Q, Shen L., Zhang J., Zheng J. “miR-647 and miR-1914 promote cancer progression equivalently by downregulating nuclear factor IX in colorectal cancer.” *Mol Med Rep.*, 2017: 6: 8189-8199.

Lu Z, Klem AM, Ramu Y “Ion conduction pore is conserved among potassium channels.” *Nature*, 413 (2001), pp. 809-813

Ludwig A, Zong X, Jeglitsch M, et al. “A family of hyperpolarization-activated mammalian cation channels.” *Nature,* 393 (1998), pp. 587-591

Malan V, Rajan D, Thomas S. “Distinct effects of allelic NFIX mutations on nonsense-mediated mRNA decay engender either a Sotos-like or a Marshall-Smith syndrome.” *Am J Hum Genet.*, 2010: 87: 189-198.

Mangoni ME, Couette B, Marger L, Bourinet E, Striessnig J, Nargeot J. “Voltage-dependent calcium channels and cardiac pacemaker activity: from ionic currents to genes.” *Prog Biophys Mol Biol.*, 2006: Jan-Apr;90(1-3):38-63. Epub 2005 Jun 6.

Mangoni ME, Couette B, Bourinet E, Platzer J, Reimer D, Striessnig J, Nargeot J. “Functional role of L-type Cav1.3 Ca2+ channels in cardiac pacemaker activity.” *Proc Natl Acad Sci U S A.*, 2003: Apr 29;100(9):5543-8. Epub 2003 Apr 16.

Mangoni ME, Nargeot J. “Properties of the hyperpolarization-activated current (I(f)) in isolated mouse sino-atrial cells.” *Cardiovasc Res.* , 2001: 51-64.

Marger L, Mesirca P, Alig J, Torrente A, Dubel S, Engeland B, Kanani S, Fontanaud P, Striessnig J, Shin HS, Isbrandt D, Ehmke H, Nargeot J, Mangoni ME. “Functional roles of Ca(v)1.3, Ca(v)3.1 and HCN channels in automaticity of mouse atrioventricular cells: insights into the atrioventricular pacemaker mechanism.” *Channels (Austin).* , 2011: May-Jun;5(3):251-61. Epub 2011 May 1.

Matuzelski E, Bunt J, Harkins D, Lim JWC, Gronostajski RM, Richards LJ, Harris L, Piper M. “Transcriptional regulation of Nfix by NFIB drives astrocytic maturation within the developing spinal cord.” *Dev Biol*, 2017: 15;432(2):286-297.

McRory JE, Hamid J, Doering CJ, Garcia E, Parker R, Hamming K, Chen L, Hildebrand M, Beedle AM, Feldcamp L, Zamponi GW, Snutch TP. “The CACNA1F gene encodes an L-type calcium channel with unique biophysical properties and tissue distribution.” *J Neurosci.*, 2004: Feb 18;24(7):1707-18.

Mermod NO, Neill E, Kelly T, Tjian R. “The proline-rich transcriptional activator of CTF/NF-1 is distinct from the replication and DNA binding domain.” *Cell*, 1989: 58, 741-753.

Mesirca P, Torrente A, Mangoni ME. “T-type channels in the sino-atrial and atrioventricular pacemaker mechanism” *Eur J Physiol*, 2014: 466:791–799.

Messina G, Biressi S, Monteverde S, Magli A, Cassano M, Perani L, Roncaglia E, Tagliafico E, Starnes L, Campbell CE, Grossi M, Goldhamer DJ, Gronostajski R.M., Cossu G. “Nfix regulates fetal-specific transcription in developing skeletal muscle.” *Cell*, 2010: Cell 140, 554–566,.

Milanesi R, Baruscotti M, Gnecchi-Ruscone T, DiFrancesco D. “Familial sinus bradycardia associated with a mutation in the cardiac pacemaker channel.” *N Engl J Med*., 2006: Jan 12;354(2):151-7.

Mitchell JA, Lye SJ. “Differential expression of activator protein-1 transcription factors in pregnant rat myometrium.” *Biol Reprod.*, 2002: 67(1):240-6.

Mommersteeg MT, Hoogaars WM, Prall OW, de Gier-de Vries C, Wiese C, Clout DE, Papaioannou VE, Brown NA, Harvey RP, Moorman AF, Christoffels VM. “Molecular pathway for the localized formation of the sinoatrial node.” *Circ Res*, 2007: Feb 16;100(3):354-62. Epub 2007 Jan 18.

Mommersteeg MT, Domínguez JN, Wiese C, Norden J, de Gier-de Vries C, Burch JB, Kispert A, Brown NA, Moorman AF, and Christoffels VM. “The sinus venosus progenitors separate and diversify from the first and second heart fields early in development.” *Cardiovasc Res*, 2010; 87:92–101.

Moorman AF e Christoffels VM. “Cardiac chamber formation: development, genes, and evolution.” *Physiol Rev*, 2003; 83(4):1223-67.

Moorman A, Webb S, Brown NA, Lamers W, Anderson RH. “Development of the heart: (1) formation of the cardiac chambers and arterial trunks.” *Heart,* 2003; Jul;89(7):806-14.

Moosmang S, Stieber J, Zong X et al. “Cellular expression and functional characterization of four hyperpolarization-activated pacemaker channels in cardiac and neuronal tissues.” *Eur J Biochem*, 2001: 1646-1652.

Ng WA, Grupp IL, Subramaniam A, Robbins J. “Cardiac Myosin Heavy Chain mRNA Expression and Myocardial Function in the Mouse Heart.” *Circulation Research*, 1991: Vol 68, No 6 1742-1750.

Nielsen M.S., Axelsen L.N., Sorgen P.L., Verma V., Delmar D., Holstein-Rathlou NK. “Gap Junctions.” *Compr Physiol.*, 2013: 10.1002/cphy.c110051.

Openstax College “Anatomy & Physiology” by Rice University, 2013.

Pape HC. “Queer current and the pacemaker: hyperpolarization-activated cation current in neurons.” *Annu Rev Physiol.*, 1996: 58:299-327.

Piper M, Barry G, Hawkins J, Mason S, Lindwall C, Little E, Sarkar A, Smith AG, Moldrich RX, Boyle GM, Tole S, Gronostajski RM, Bailey TL, Richards LJ. “NFIA controls telencephalic progenitor cell differentiation through repression of the Notch effector Hes1.” *Neurosci*, 2010: 30:9127–9139.

Piper M, Harris L, Barry G, Heng YH, Plachez C, Gronostajski RM, Richards LJ. “Nuclear factor one X regulates the development of multiple cellular populations in the postnatal cerebellum.” *J Comp Neurol*, 2011: 519:3532–3548.

Platzer J, Engel J, Schrott-Fischer A, Stephan K, Bova S, Chen H, Zheng H, Striessnig J. “Congenital deafness and sinoatrial node dysfunction in mice lacking class D L-type Ca2+ channels.” *Cell*, 2000: Jul 7;102(1):89-97.

Priolo M, Schanze D, Tatton-Brown K, Mulder PA, Tenorio J, Kooblall K, Acero IH, Alkuraya FS, Arias P, Bernardini L, Bijlsma EK, Cole T, Coubes C, Dapia I, Davies S, Di Donato N, Elcioglu NH, Fahrner JA, Foster A, González NG. “Further delineation of Malan syndrome.” *Hum Mutat.*, 2018: doi: 10.1002/humu.23563.

Qu J, Altomare C, Bucchi A, DiFrancesco D, Roinson RB. “Functional comparison of HCN isoforms expressed in ventricular and HEK 293 cells.” *Eur J Physiol*, 2002: 444: 597. https://doi.org/10.1007.

Rahman NIA., Abdul Murad NA., Mollah MM., Jamal R, Harun R. “NFIX as a Master Regulator for Lung Cancer Progression.” *Front Pharmacol.*, 2017: 8:540.

Robinson RB, Siegelbaum SA. “Hyperpolarization-activated cation currents: from molecules to physiological function.” *Annu Rev Physiol*,, 2003: 453-480.

Robinson RB, Yu H, Chang F, Cohen IS. “Developmental change in the voltage-dependence of the pacemaker current, if, in rat ventricle cells.” *Pflugers Arch.* , 1997: 533-5.

Rosa JM, Nanclares C, Orozco A, Colmena I, de Pascual R, García AG, Gandía L. “Regulation by L-type calcium channels of endocytosis: an overview.” *J Mol Neurosci.* , 2012: 360-7.

Rose RA, Sellan M, Simpson JA, Izaddoustdar F, Cifelli C, Panama BK, Davis M, Zhao D, Markhani M, Murphy GG, Striessnig J, Liu PP, Heximer SP, Backx PH. “Iron overload decreases CaV1.3-dependent L-type Ca2+ currents leading to bradycardia, altered electrical conduction, and atrial fibrillation.” *Circ Arrhythm Electrophysiol.* , 2011: Oct;4(5):733-42. doi: 10.1161/CIRCEP.110.960401. Epub 2011 Jul 11.

Rossi G, Antonini S, Bonfanti C, Monteverde S, Vezzali C, Tajbakhsh S, Cossu G, Messina G. “Nfix Regulates Temporal Progression of Muscle Regeneration through Modulation of Myostatin Expression.” *Cell Reports*, 2016: 14, 2238–2249.

Rossi G, Bonfanti C, Antonini S, Bastoni M, Monteverde S, Innocenzi A, Saclier M, Taglietti V, Messina G. “Silencing Nfix rescues muscular dystrophy by delaying muscle regeneration.” *Nat Commun.*, 2017: 8(1):1055.

Saito Y, Nakamura K, Yoshida M, Sugiyama H, Ohe T, Kurokawa J, Furukawa T, Takano M, Nagase S, Morita H, Kusano KF, Ito H. “Enhancement of Spontaneous Activity by HCN4 Overexpression in Mouse Embryonic Stem Cell-Derived Cardiomyocytes - A Possible Biological Pacemaker.” *Plos One*, 2015: 10(9):e0138193. doi: 10.1371/journal.pone.0138193. eCollection 2015.

Santoro B, Grant SGN, Bartsch D, Kandel ER. “Interactive cloning with the SH3 domain of N-src identifies a new brain specific ion channel

protein, with homology to Eag and cyclic nucleotide-gated channels." *PNAS*, 1997: pp. 14815-14820.

Santoro B, Liu DT, Yao H et al. "Identification of a gene encoding a hyperpolarization-activated pacemaker channel of brain." *Cell*, 93 (1998), pp. 717-729

Scavone A, Capilupo D.,Mazzocchi N, Crespi A, Zoia S, Campostrini G, Bucchi A, Milanesi R, Baruscotti M, Benedetti S, Antonini S, Messina G, DiFrancesco D, Barbuti A. "Embryonic Stem Cell-Derived CD166+ Precursors Develop into Fully Functional Sinoatrial-Like Cells." *Circulation Research*, 2013: Volume 123, Issue 1.

Sinnegger-Brauns MJ, Hetzenauer A, Huber IG, Renström E, Wietzorrek G, Berjukov S, Cavalli M, Walter D, Koschak A, Waldschütz R, Hering S, Bova S, Rorsman P, Pongs O, Singewald N, Striessnig J. "Isoform-specific regulation of mood behavior and pancreatic beta cell and cardiovascular function by L-type Ca 2+ channels." *J Clin Invest.*, 2004: May;113(10):1430-9.

Striessnig, J. "Pharmacology, structure and function of cardiac L-type Ca(2+) channels." *Cell Physiol Biochem.*, 1999: 242-69.

Taglietti V, Maroli G, Cermenati S, Monteverde S, Ferrante A, Rossi G, Cossu G, Beltrame M, Messina G. "Nfix Induces a Switch in Sox6 Transcriptional Activity to Regulate MyHC-I Expression in Fetal Muscle." *Cell Rep.*, 2016: 17(9):2354-2366.

Tanabe T, Beam KG, Powell JA, Numa S. "Restoration of excitation–contraction coupling and slow calcium current in dysgenic muscle by dihydropyridine receptor complementary DNA." *Nature*, 1988: Nov 10;336(6195):134-9.

Ulens C and Siegelbaum SA. “Regulation of Hyperpolarization-Activated HCN channels by cAMP through a gating switch in binding domain symmetry.” *Neuron*, 2003: Volume 4, Issue 5, 959-970.

Verkerk AO, Wilders R, van Borren MM, Peters RJ, Broekhuis E, Lam K, Coronel R, de Bakker JM, Tan HL. “Pacemaker current (If) in the human sinoatrial node.” *Eur. Heart J.*, 2007: :2472-8.

Vidovic D, Davila RA, Gronostajski RM, Harvey TJ, Piper M. “Transcriptional regulation of ependymal cell maturation within the postnatal brain.” *Neural Dev*, 2018: 16;13(1):2.

Vidovic D, Harris L, Harvey TJ, Evelyn Heng YH, Smith AG, Osinski J, Hughes J, Thomas P, Gronostajski RM, Bailey TL, Piper M. “Expansion of the lateral ventricles and ependymal deficits underlie the hydrocephalus evident in mice lacking the transcription factor NFIX.” *Brain Res.*, 2015: 1616:71-87.

Vinogradova TM, Zhou YY, Bogdanov KY, Yang D, Kuschel M, Cheng H, Xiao RP. “Sinoatrial node pacemaker activity requires Ca2+/calmodulin-dependent protein kinase II activation-.” *Circulation Research*, 2000: Oct 27;87(9):760-7.

Wang P, Tang M, Gao L, Luo H, Wang G, Ma X, Duan Y. “Roles of I(f) and intracellular Ca2+ release in spontaneous activity of ventricular cardiomyocytes during murine embryonic development.” *J Cell Biochem.* , 2013: 1852-62.

Xu W, Lipscombe D. “Neuronal Ca(V)1.3alpha(1) L-type channels activate at relatively hyperpolarized membrane potentials and are incompletely inhibited by dihydropyridines.” *J Neurosci.* , 2001: Aug 15;21(16):5944-51.

Zagotta WN, Olivier NB, Black KD, Young EC, Olson R. Gouaux. "Structural basis for modulation and agonist specificity of HCN pacemaker channels." *Nature*, 2003: 425(6954):200-5.

Zhou Y, Morais-Cabral JH, Kaufman A, MacKinnon R "Chemistry of ion coordination and hydration revealed by a K+ channel-Fab complex at 2.0 Å resolution." *Nature*, 414 (2001), pp. 43-48